Clays and Clay Minerals, Vol. 69, No. 2:167–187, 2021

ION-EXCHANGE MODELING OF DIVALENT CATION ADSORPTION ON SWy-3 MONTMORILLONITE

Yayu W. Li[1,*] and Cristian P. Schulthess[1]
[1] Department of Plant Science and Landscape Architecture, University of Connecticut, Storrs, CT 06269-4067, USA

Abstract—Ion-exchange modeling is used widely to describe and predict ion-adsorption data on clay minerals. Although the model parameters are usually optimized by curve fitting experimental data, this approach does not confirm the identity of the adsorption sites. The purpose of the present study was to extend to divalent cations a previous study on the retention of monovalent cations on Na-saturated montmorillonite (NaMnt) which optimized some of the model parameters using density functional theory (DFT) simulations. The adsorption strength of divalent cations increased in the order $Mg^{2+} < Cd^{2+} < Ca^{2+} < Sr^{2+} < Ba^{2+}$. After adding adsorption of metal hydroxide species (MOH^{+}), the three-site ion-exchange model was able to describe adsorption data over a wide pH range (pH 1–10) on NaMnt. X-ray diffraction (XRD) analyses were conducted to investigate the interlayer dimension of clay samples under various conditions. The cation retention strengths of divalent cations did not correlate with interlayer dimensions. The XRD analyses of the Mnt showed a d_{001} value of 19.6 Å when saturated with alkaline earth cations, 22.1 Å with Cd^{2+}, 15.6 Å with Na^{+}, and 15.2 Å with H^{+}. In the case of Na^{+}, the 15.6 Å peak decreased gradually and disappeared, and new peaks at 22.1 and 19.6 Å appeared when the percentages of Mg^{2+} and Ba^{2+} adsorbed increased on NaMnt. The peak shifted from 22.1 to 20.3 and 19.6 Å when the pH increased for all cations except Cd^{2+}, which stayed constant at 22.1 Å. The coexistence of multiple d_{001} peaks in the XRD patterns suggested that the interlayer cations were segregated, and that the interlayer ion–ion interactions among different types of ions were minimized.

Keywords—Adsorption envelope · Adsorption equilibrium constant · Alkaline earth cation · Ion-exchange model · Montmorillonite · Octahedral cation distribution · X-ray diffraction

INTRODUCTION

Montmorillonite (Mnt) is one of the most important components in soils and clays for the adsorption of cations due to its large cation exchange capacity (CEC). It is often also used as a barrier in disposal sites due to its abundance and low price (Reijonen and Alexander 2015; Milodowski et al. 2016). Understanding the adsorption mechanism of divalent cations on Mnt helps to explain their transportation and fate in the environment.

Most inorganic soil nutrients and contaminants can dissolve in water and exist as ions. Their adsorption and desorption on the solid phase play a significant role in their availability and fate in the environment, which, in turn, impacts environmental health and safety. Divalent alkaline earth cations are abundant in the earth's crust, ranging from 0.025% for Ba to 3.63% for Ca (Fleischer 1953). The divalent Mg^{2+} and Ca^{2+} cations are essential plant nutrients (Jones 2012). The ^{90}Sr isotope which is radioactive, with a half-life of 28 years (Lagoutine et al. 1978), can enter the environment via wastewater from nuclear power plants, from the fallout from nuclear weapons testing, or from nuclear accidents (Libby 1956). The Sr^{2+} cations have similar properties to Ca^{2+} cations, so Sr^{2+} will substitute readily for Ca^{2+} in the food chain and be deposited in the bones of mammals that consume it (Starichenko 2011). The emission of beta particles from ^{90}Sr can result in tumors (Nilsson and Book 1987). Although the Ba^{2+} cation has a wide application in industry, high levels of Ba^{2+} have caused serious environmental problems from mining (Kravchenko et al. 2014). The divalent alkaline earth cations are in the same column in the periodic table of elements and have similar electron configurations (all subshells are filled and end with s^2, which are easily lost). These cations should, therefore, follow similar reaction processes when reacting with soil components.

The Cd^{2+} cation is ubiquitous in nature from weathering of rocks and its anthropogenic source is increasing due to its industrial applications (Pinot et al. 2000). The Cd^{2+} cation is a highly soluble and mobile divalent heavy metal in the environment (Cullen and Maldonado 2013). High levels of Cd^{2+} can accumulate in the human body and cause serious health issues (Nordberg 2004). The Cd^{2+} cation is a transition metal and its electron configuration is $[Kr]4d^{10}5s^2$, where the s^2 subshell is easily lost. In this regard, it is very similar to the alkaline earth metals, and should, therefore, follow reaction processes with soil components which are similar to those of the alkaline earth cations.

Ion-exchange models have been shown to be useful tools to describe and predict cation adsorption on soil constituents over a wide range of chemical conditions (Table 1). The ion-exchange models are essentially macroscopic models that consider the overall sorption properties of mineral phases based on charge-balance principles, and do not consider any intrinsic assumptions on the nature of the surface

* E-mail address of corresponding author: yayu.li@uconn.edu
DOI: 10.1007/s42860-021-00115-y
© The Clay Minerals Society 2021

https://doi.org/10.1007/s42860-021-00115-y Published online by Cambridge University Press

Table 1 Literature review of ion-exchange models for divalent cation adsorption on soil minerals

Adsorbent	Divalent cations	Number of sites	Method to obtain CEC and number of sites	References
Argillite	Mg, Ca	3, 4, or 5	Adsorption isotherm and envelope	Jacquier et al. (2004)
Beidellite	Mg, Ca, Ra	3	Adsorption isotherm and envelope	Robin et al. (2015, 2017)
Bentonite	Mg, Ca	1	Adsorption isotherm	Klika et al. (2007)
Bentonite	Mg, Ca	2	Adsorption isotherm	Missana et al. (2014)
Bentonite	Sr	3	From Nolin (1997)	Siroux et al. (2017)
Bentonite, illite	Ca	4	From Nolin (1997)	Martin et al. (2018)
Bentonite, Clayey sandstone, Illite	Ca, Sr	4	From Nolin (1997) and Peynet (2003)	Wissocq et al. (2018)
Clayey rock	Mg, Ca	3	Adsorption envelope	Motellier et al. (2003)
Clayey rock	Mg, Ca, Sr	3	From Nolin (1997)	Savoye et al. (2015)
Montmorillonite	Ca	3	Adsorption envelope	Peynet (2003)
Montmorillonite	Mg, Ca, Sr, Ba	1	Adsorption isotherm	Laudelout et al. (1968)
Montmorillonite	Ca	1 or 3	From Nolin (1997)	Tertre et al. (2011)
Natural soil and sediment	Mg, Ca, Zn	4	From Nolin (1997)	Tertre et al. (2009)
Vermiculite	Ca, Sr	2	Adsorption isotherm	Dzene et al. (2016)

interactions. Ion-exchange models can describe and predict the sorption of both major and trace elements in a system.

The number of adsorption sites and the CEC of each site are essential parameters of ion-exchange models. The optimization of these two parameters was based normally on the model fitting of cation adsorption data, and thus can vary greatly in the literature for similar minerals (Table 1). Cation adsorption data were collected commonly as a function of pH (adsorption envelopes) or cation concentration (adsorption isotherms). For example, the number of adsorption sites in some studies was taken from the number of edges in the adsorption envelope curve and the CEC of each site from their adsorption maxima (Motellier et al. 2003; Jacquier and Beaucaire 2004; Robin et al. 2015, 2017). Some other studies obtained directly the number of adsorption sites and the CEC of each site from the Na^+ adsorption envelope curve of Nolin's (1997) Na^+ adsorption envelope curve (Savoye et al. 2015; Siroux et al. 2017; Wissocq et al. 2018).

Reducing the number of unknown parameters in ion-exchange models reduces their dependence on the curve-fitting exercise and increases the certainty of the models. Alkali cation adsorption data on Mnt were described successfully (Li and Schulthess 2020) using an ion-exchange model that used pre-determined model parameters (i.e. number of adsorption sites and relative CEC percentage on each site) from an independent Density Functional Theory simulation (DFT; Li et al. 2020). Three types of interlayer adsorption sites with distinctive H^+ adsorption strengths were found on Mnt based on the Fe–Mg distance in cations in the octahedral sheets. The relative CEC of each of these three types of sites corresponded to the probability of formation of their octahedral Fe–Mg distances. With the independently calculated number of adsorption sites and relative CEC of these three sites, a three-site ion-exchange model was developed to describe successfully monovalent cation adsorption data on Mnt. This model was able to describe Cs^+ adsorption isotherm data, as well as the retention of various mixtures of monovalent cations in pH-dependent adsorption envelopes.

The current study aimed to test the validity of the ion-exchange model developed by Li and Schulthess (2020) for predicting divalent cation adsorption on Mnt. In other words, it sought to test an ion-exchange model for the retention of divalent cations based on three interlayer sites with the same relative CEC of each site that was developed previously for monovalent ions. The study also sought to investigate the relation between cation adsorption strength and the clay's interlayer space, which was previously observed with monovalent cations (Li and Schulthess 2020).

MATERIALS AND METHODS

Na, Mg, Ca, Sr, Ba, and Cd-saturated Montmorillonite

The same NaMnt sample from Li and Schulthess (2020) was used in the present study. The NaMnt was prepared by mixing SWy-3 Mnt (from the Source Clays Repository of The Clay Minerals Society) with 0.01 mol/L HCl for 12 h, centrifuging at 29,900×*g* and 20°C for 5 min, decanting the

https://doi.org/10.1007/s42860-021-00115-y Published online by Cambridge University Press

supernatant, adding 1 mol/L NaCl solution, and resuspending the clay sediment. This procedure was carried out eight times using 1 mol/L NaCl solutions, followed by washing with deionized water a further eight times to remove the excess NaCl salt and to reach neutral pH conditions. These steps were performed in centrifuge tubes using 2 g of clay with 30 mL of liquid in each tube. Some of the smaller clay particles were lost with decanted supernatants when the clay was washed with deionized water; no loss of clay sample was observed in subsequent steps. The final NaMnt clay suspension was then diluted with deionized water to 4 L and pH 6.7.

The solids concentration in the NaMnt stock suspension was 21.30 g/L. The dry clay samples were analyzed at high temperatures. A supernatant aliquot was first oven-dried at 80°C for 12 h, followed by heating at a rate of 10°C/min up to 800°C under an argon atmosphere and analyzed using thermogravimetric analysis (TGA Q500, TA Instruments, New Castle, Delaware, USA). The 21.30 g/L clay concentration value was based on the dry clay weight at the temperature of 178°C, from which all the interlayer water had been removed (Bala et al. 2000; Tajeddine et al. 2015).

The Mg-, Ca-, Sr-, Ba-, and Cd-saturated Mnt samples (designated MgMnt, CaMnt, SrMnt, BaMnt, and CdMnt, respectively) were prepared using the same procedure as employed by Li and Schulthess (2020) starting with NaMnt. Aliquots of 30 mL of NaMnt clay suspension were centrifuged at 29,900×*g* and 20°C for 5 min, and the supernatant decanted. The resultant clay sediments were then mixed with 20 mL of corresponding 1 mol/L solutions of $MgCl_2$, $CaCl_2$, $SrCl_2$, $BaCl_2$, or $CdCl_2$ for 12 h, centrifuged at 29,900×*g* and 20°C for 5 min, the supernatant decanted, new solution added, and the clay sediment resuspended to 30 mL. This procedure was carried out eight times, followed by washing with deionized water a further eight times to remove the excess salt. On the eighth time, the clay suspensions saturated with corresponding cations were centrifuged at 29,900×*g* and 20°C for 30 min to compact the clay samples more completely, the supernatants were decanted, and no losses of clay samples were observed. The resulting clay sediments were water-saturated and analyzed using X-ray diffractometry, as discussed below.

Cation Adsorption Envelopes

Stock solutions of $MgCl_2$, $CaCl_2$, $SrCl_2$, $BaCl_2$, and $CdCl_2$ (30 mmol/L each) and NaOH (56 mmol/L) were prepared using reagent-grade chemicals. In the adsorption envelope experiments, the clay suspension and solutions were added as follows: into 50-mL nominal Oak Ridge centrifuge tubes (Thermo Fisher Scientific, Boston, Massachusetts), 9.0 mL of clay suspension was mixed with variable amounts of distilled water, and variable amounts of 0.01, 0.05, or 2 mol/L HCl for pH adjustment; 0.5 mL of 56 mmol/L NaOH was then added for fixed competitive Na^+ concentrations, followed by 3.0 mL of the corresponding salt solutions ($MgCl_2$, $CaCl_2$, $SrCl_2$, $BaCl_2$). The total volume in each tube was 30 mL. Similar procedures were conducted for $CdCl_2$ adsorption envelopes but using 10.0 mL of clay suspension and 4.6 mL of $CdCl_2$ solution instead. The initial conditions for various cation-adsorption reactions are listed in Table 2

All the batch suspensions were mixed for 20 h at 25 ± 2°C, centrifuged at 29,900×*g* and 20°C for 30 min, and the supernatant solution analyzed for remaining aqueous cation concentrations and pH. The cation concentrations were analyzed using inductively coupled plasma-atomic emission spectroscopy (ICP-AES, Spectro Ciros, Kleve, Germany). Aqueous equilibrium pH was measured using a Thermo Scientific Orion 2-Star Benchtop pH Meter.

The amounts of cations adsorbed were obtained by subtracting the remaining aqueous cation concentration from the total initial cation concentration. A propagation-of-error analysis was performed on all the adsorption data. The ion-exchange model parameters were optimized using *IExfit* software (version 3.3, www.alfisol.com). Ionic activities of aqueous ions were calculated using the Davies equation (Davies 1938). The goodness-of-fit pseudo-R^2 values of the optimization results are Efron's pseudo-R^2 values (Efron 1978), which is used commonly for non-linear regression studies. The stability constants of the aqueous reactions were from the National Institute of Standards and Technology database (NIST 46.8; www.nist.gov/srd/nist46).

X-ray Diffraction Analysis

The d_{001} values of wet clay samples from centrifugation containing various cations were measured at room temperature using XRD analysis (D2 Phaser, Bruker Corp.,

Table 2 The initial conditions for cation-adsorption reactions. The Cl^- concentration varied due to the addition of HCl for pH adjustments. The pH values are shown in parentheses after the minimum and maximum ionic-strength values

Adsorption envelope	Clay conc. (g/L)	Total ion concentration (mmol/L)							Ionic strength (mmol/L) and pH
		Na^+	Mg^{2+}	Ca^{2+}	Sr^{2+}	Ba^{2+}	Cd^{2+}	Cl^-	
Mg-NaMnt	6.46	5.44	3.03					6.00–172.67	6.65 (9.44)–157.42 (0.9)
Ca-NaMnt	6.46	5.44		3.00				6.00–172.67	6.80 (9.67)–157.34 (0.9)
Sr-NaMnt	6.46	5.44			3.00			6.00–172.67	6.79 (9.59)–155.81 (0.91)
Ba-NaMnt	6.46	5.44				3.00		6.00–172.67	6.78 (9.74)–155.69 (0.91)
Cd-NaMnt	7.10	5.74					4.60	9.32–142.53	11.44 (7.26)–130.86 (0.95)

https://doi.org/10.1007/s42860-021-00115-y Published online by Cambridge University Press

Madison, Wisconsin, USA). The XRD was equipped with a powder diffractometer with CuKα radiation (wavelength = 1.54184 Å), graphite monochromator, and a LynxEye linear detector. The centrifuged wet clay samples from the cation adsorption envelopes and Mg-, Ca-, Sr-, Ba-, Cd-saturated samples were put in a Si low-background sample holder (Bruker Corp.) using a spatula and leveled with a glass slide. Data were collected from 2 or 5–12°2θ with a 0.02°2θ step size and a count time of 0.5 s per step. The weights of these clay pastes were recorded before and after XRD analysis to examine the losses of water from the clay during the analysis process. The water loss was negligible (<0.3%). The influence of clay water content on the XRD d_{001} values was tested with a batch analysis of SWy-3 samples with water contents ranging from 70 to 86% equilibrated for 90 h. The XRD peak intensities decreased with increasing water content, and the d_{001} values increased by 1 Å. The clay samples from the cation adsorption envelope and isotherm experiments had a water-content range of 70–78% (equivalent to 2.33–3.55 g of water per g of dry clay sample), which corresponds to a variability of 0.2 Å for the d_{001} value.

RESULTS AND DISCUSSION

Mineral Stability and Cation Exchange Capacity

The same SWy-3 and NaMnt samples were used in the present study as in that by Li and Schulthess (2020). The XRD analysis showed small amounts of feldspar, illite, and quartz impurities in the SWy-3 and NaMnt samples. The CEC values of feldspar (2.8–20 μmol/g, Nash and Marshall 1956), illite (75–240 μmol/g, Baeyens and Bradbury 2004), and quartz (0 μmol/g) are much smaller than Mnt (764 μmol/g, The Clay Minerals Society 2020). Accordingly, the primary mineral contributing to the CEC of NaMnt was Mnt, and the model development treated the NaMnt as pure Mnt. Very low concentrations of K^+, Ca^{2+}, and Mg^{2+} cations existed in the NaMnt sample after the Na-saturation procedures, and the equivalent charge of these three types of cations was 1.68% of the total Na^+ in the sample (712.8 ± 1.7 μmol/g, Li and Schulthess 2020). The removal of cations from clay minerals was suggested to be very difficult when working with SWy-1 Mnt (Baeyens and Bradbury 1997). Na^+, K^+, and Ca^{2+} cations were found in Cu-trien- or alkylammonium-saturated smectites (clay sources not provided) by Kaufhold et al. (2011), who suggested that these cations came from undetected traces of feldspar or volcanic glass. The K^+, Ca^{2+}, and Mg^{2+} cations in the NaMnt were not considered in the present study due to the small amounts. Accordingly, Na^+ was the only dominant exchangeable cation in NaMnt.

The aqueous Al^{3+} and Fe^{3+} concentrations were analyzed to examine the dissolution of clay minerals at low pH. The aqueous Al^{3+} and Fe^{3+} concentrations increased as the pH decreased below pH 5 and 4, respectively. If the aqueous Al^{3+} and Fe^{3+} cations came from the dissolution of clay minerals, the dissolution and re-adsorption of these autochthonous Al^{3+} and Fe^{3+} ions result essentially in a restructuring of clay surface sites. Based on the chemical formula of NaMnt and the aqueous Al^{3+} and Fe^{3+} concentrations, the greatest dissolution rates of NaMnt in the presence of various divalent cations were estimated to be 0.05% and 1.03%, respectively (data not shown). If some of the aqueous Al^{3+} and Fe^{3+} cations came from the detachment of colloids, as observed by Kaufhold and Dohrmann (2008) for 38 different types of bentonite samples, then the clay dissolution rates were less than the above-predicted values. Accordingly, clay dissolution was not included in adsorption modeling because of the low aqueous Al^{3+} and Fe^{3+} concentrations and the low estimate on clay dissolution.

Ion-Exchange Modeling

The development of an adsorption model for divalent cations should be a consistent and logical continuation of models developed for monovalent cations on the same mineral. Specifically, the number of adsorption sites, the CEC of each site, and cation adsorption strength should be the same for both models. Using DFT simulations, three types of adsorption sites with distinctive H^+ adsorption strengths were identified on Mnt based on their octahedral Fe-Mg cation distribution (Li et al. 2020). All three sites were interlayer sites, and their relative CEC can be calculated based on the statistical probabilities of their octahedral Fe-Mg cation distributions. Accordingly, three types of adsorption sites and their relative CECs were identified on NaMnt, and a three-site ion-exchange model was developed successfully to describe the adsorption of monovalent alkali cations on NaMnt (Li and Schulthess 2020). To maintain consistency of the nature of adsorption sites on NaMnt, a similar three-site ion-exchange model was developed here to predict divalent cation adsorption on NaMnt.

In the adsorption study of monovalent alkali cations, the maximum amount of cations adsorbed on NaMnt was 710 μmol/g (Li and Schulthess 2020). The same value was observed in the adsorption of divalent cations around pH 6 in the present study (Fig. 1). The amount of cations adsorbed remained constant in the study of monovalent alkali cations when the pH was >6, however, but continued to increase with increasing pH in Fig. 1. The difference in the adsorption behavior at high pH will be discussed further in the next section. For now, this section focuses on cation adsorption at pH < 6 using an ion-exchange model that is similar to that developed by Li and Schulthess (2020). The probabilities of different octahedral cation distributions in NaMnt were ~43, ~43, and ~14%. Accordingly, the CEC of three interlayer sites (S_a, S_b, and S_c) were calculated as 305, 305, and 100 μmol/g with 710 μmol/g as the total CEC of NaMnt. The H^+ cation was considered to be the reference cation for the presentation of all cation adsorption equilibrium constants due to its prevalence in aqueous ion-exchange reactions. Accordingly, the M^{2+}-H^+-Na^+ competitive ion-exchange reactions on site S_i (i=a, b, or c) were:

$$S_iH + Na^+ \rightleftharpoons S_iNa + H^+ \quad (1)$$

https://doi.org/10.1007/s42860-021-00115-y Published online by Cambridge University Press

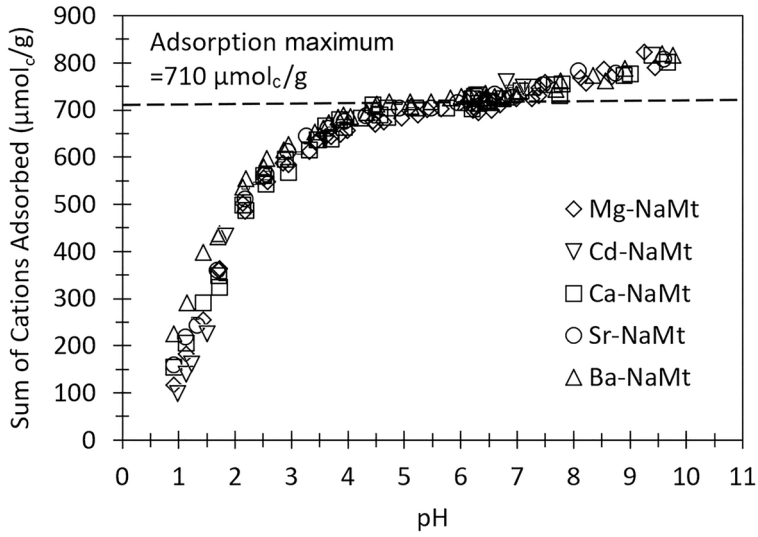


Fig. 1 The sum of equivalent charge of adsorbed cations on NaMnt for various conditions. The largest error was ±6.95 µmol/g

$$2S_iH + M^{2+} \rightleftharpoons (S_i)_2M + 2H^+ \quad (2)$$

where M^{2+} was the Cd^{2+}, Mg^{2+}, Ca^{2+}, Sr^{2+}, or Ba^{2+} divalent cation. The corresponding equilibrium constants were defined as products over reactants:

$$K_{i,Na} = \frac{\{S_iNa\}(H^+)}{\{S_iH\}(Na^+)} \quad (3)$$

$$K_{i,M} = \frac{\{(S_i)_2M\}(H^+)^2}{\{S_iH\}^2(M^{2+})} \quad (4)$$

where { } represents the concentration of adsorbed cations on the solid surface, and ( ) represents the aqueous ionic activities. The known adsorption maximum (Γ_{max}) for each site was equal to the sum of adsorbed H^+, Na^+, and divalent cations:

$$\Gamma_{max,Si} = \{S_iH\} + \{S_iNa\} + 2\{(S_i)_2M\} \quad (5)$$

The equilibrium constants for each cation are a result of the chemical energy in two environments: (1) the hydration energy in the liquid phase, which is relatively constant in the bulk solution, but may vary in the interlayer (referred to as the subaqueous interlayer phase by Teppen and Miller 2006); and (2) the adsorption energy of the surface sites. If all possible ion–ion interactions are relatively constant in the interlayer region, then the cation equilibrium constants (or adsorption strength) should be consistent for each specific mineral and cation. The negative logarithm of adsorption strength (pK) of Na^+ on each site of NaMnt was, therefore, kept the same as the values from the previous study of alkali cation adsorption on NaMnt (Li and Schulthess 2020). This assumption is discussed further in the XRD analysis section below. The only unknown parameters were the K constants for the adsorption of divalent cations (M^{2+}) on the three interlayer sites (S_a, S_b, and S_c in Table 3a) on NaMnt, which were optimized based on the curve fit of the experimental adsorption envelopes. The optimization results showed that the three-site ion-exchange model was able to simulate the cation adsorption data very well for all cation adsorption envelope data below pH 6 (Fig. 2).

The divalent cations can form MCl^+ complexes in a Cl-rich medium. Several studies have confirmed the adsorption of MCl^+ ion pairs in the interlayer of Mnt. For example, the coexistence of Cd^{2+} and $CdCl^+$ in the interlayers of Mnt (Cornwall, UK) equilibrated with high concentrations (>0.2 N) of $CdCl_2$ solutions was revealed by Di Leo and Cuadros (2003) using nuclear magnetic resonance. Using XRD and 77 K Mössbauer spectroscopy analysis in cation exchange experiments on MX-80 Mnt, Tournassat et al. (2004a, 2004b) concluded that $CaCl^+$ participated in ion-exchange reactions when the $CaCl_2$ concentrations were 6.8 and 50 mM, and the clay contents were 3.03 and 1.53 g/L, respectively. Using an XRD profile modeling approach, the existence of $MgCl^+$, $CaCl^+$, or $SrCl^+$ ion pairs in the interlayer of divalent cation-saturated SWy-2 Mnt with large metal-Cl^+ concentrations of 1 M was suggested by Ferrage et al. (2005b). Cation adsorption isotherm data on MX-80 Mnt were predicted, including $FeCl^+$, $CaCl^+$, and $MgCl^+$ cations by Charlet and Tournassat (2005) in their ion-exchange model using a total Cl^- concentration of 49–132 mM and a pH range of 2.17–3.59. Accordingly, surface adsorption reactions for these Cl-complexes are expressed here as:

$$S_iH + M^{2+} + Cl^- \rightleftharpoons S_iMCl + H^+ \quad (6)$$

and the corresponding equilibrium constants were defined as products over reactants:

https://doi.org/10.1007/s42860-021-00115-y Published online by Cambridge University Press

Table 3 The adsorption maxima (Γ_{max}) and negative logarithm of equilibrium constants (pK) of three sites optimized with the strict ion-exchange model for **a** non-hydrolyzed and **b** hydrolyzed cations. The initial conditions of ion-exchange reactions are shown in Table 2. The term "est" indicates that the pK values were estimated. The asterisk (*) denotes that these cations are defined according to Eq. 8

	Cations	S_a	S_b	S_c
a	Na^+	–0.7	0.6	2.6
	$*Mg^{2+}$	–3.5	–1.6	1.2
	$*Cd^{2+}$	–3.5	–1.8	1.2
	$*Ca^{2+}$	–3.5	–2.0	1.1
	$*Sr^{2+}$	–3.6	–2.1	0.8
	$*Ba^{2+}$	–3.6	–2.7	0.6
b	$MgOH^+$	9 est	9 est	8.6
	$CdOH^+$	8 est	8 est	8.0
	$CaOH^+$	10 est	10 est	8.5
	$SrOH^+$	10.5 est	10.5 est	8.0
	$BaOH^+$	10.5 est	10.5 est	8.5
	Site CEC, μmol/g	305	305	100

$$K_{i,MCl} = \frac{\{S_iMCl\}(H^+)}{\{S_iH\}(M^{2+})(Cl^-)} \quad (7)$$

The retention data of Cl^- ions or MCl^+, which are needed to obtain their corresponding adsorption pK values, are missing. In the absence of data for optimizing the $K_{i,MCl}$ values, the $K_{i,MCl}$ values were combined with the $K_{i,M}$ values, where the cation concentrations are expressed as:

$$[^*M^{2+}] = [M^{2+}] + [MCl^+] \quad (8)$$

and the $K_{i,M}$ values were redefined in Eq. 4 in terms of $*M^{2+}$ rather than M^{2+}; therefore, MCl^+ was not considered explicitly in the present study. The pK values in Table 3 are a composite of the adsorption of complexed MCl^+ and non-complexed M^{2+} species. Simulations that optimized the $K_{i,M}$ values while keeping the $K_{i,MCl}$ fixed at low values (equivalent to the K values of Na^+) resulted in slightly improved predictions. Simulations which optimized the $K_{i,M}$ values while keeping the $K_{i,MCl}$ fixed at high values (about half of the $K_{i,M}$ values of M^{2+}) resulted in very poor retention predictions, however (data not shown). Thus, the retention strength of monovalent MCl^+ cations can be assumed to be much weaker than that of divalent M^{2+}, and the amount retained was very small at pH > 2 where the concentrations of Cl^- anions were lower.

The equilibrium constant pK values increased with sites $S_a < S_b < S_c$ (Table 3a), which suggested that the cation adsorption strength relative to H^+ decreased in the order $S_a > S_b > S_c$. The same cation-adsorption strength sequence of these three interlayer sites was also obtained from the adsorption studies of alkali cations on NaMnt (Li and Schulthess 2020). The pK values of divalent cations were smaller (or more negative) than those for the Na^+ cation, which meant that the cation adsorption strengths of divalent cations were stronger than for the Na^+ cation on Mnt. Greater cation-adsorption strength of divalent cations was also observed by Laudelout et al. (1968) and Berghout et al. (2010), who attributed the difference to the stronger Coulombic attraction of divalent cations on the clay minerals. The pK values of divalent cations decreased roughly in the order $Mg^{2+} > Cd^{2+} > Ca^{2+} > Sr^{2+} > Ba^{2+}$, particularly for sites S_b and S_c, which meant that the adsorption strength increased in the opposite order. A calorimetric adsorption enthalpy study of NH_4^+-M^{2+} exchange reactions on Mnt showed the same cation adsorption strength sequence: $Mg^{2+} > Ca^{2+} > Sr^{2+} > Ba^{2+}$ (Laudelout et al. 1968). The pK values reflect the affinity of cations toward the clay surface sites relative to their affinity for forming hydrated species in the interlayer liquid phase. Moderate to strong linear correlation between pK values and the hydration energy were found for both monovalent alkali and divalent alkaline earth cations (Fig. 3). Using computational molecular mechanics, the adsorption selectivity of isovalent cations was found by Teppen and Miller (20006) to be controlled by their hydration energy. The weaker the hydration energy (lower $-\Delta H^o_{hyd}$ in Table 4), the easier it is for the cations to dehydrate in the interlayer space and adsorb strongly on the clay surface.

Very few studies compared directly the adsorption strength of Cd^{2+} with alkaline earth cations, and discrepancies exist in the published studies on their adsorption strengths. Following a comprehensive literature review of published ion-exchange data on smectite, the equilibrium constants of divalent cations on Camp Berteau Mnt were compared by Benson (1980) using a one-site ion-exchange model, and showed that the cation adsorption strength relative to H^+ decreased in the order $Cd^{2+} > Ba^{2+} > Ca^{2+} > Sr^{2+} > Mg^{2+}$, but in the order $Cd^{2+} > Ba^{2+} > Mg^{2+} > Ca^{2+} > Sr^{2+}$ relative to Na^+, both of which were different from what was observed in the current study. The discrepancies proposed by Benson (1980) in the cation adsorption equilibrium constants were due to the differences in laboratory procedures and composition of the clay samples. The models proposed here, however, will also influence heavily the resultant selectivity constants. For example, the cation adsorption affinity to the Na-Mnt surface was shown by Farrah et al. (1980) to follow the order $Cd^{2+} > Mg^{2+} > Ca^{2+}$ based on the Langmuir constants, but in the order $Ca^{2+} > Mg^{2+} > Cd^{2+}$ using the competitive Langmuir equation. In the present study, the adsorption strength of Cd^{2+} was found to be between those of Mg^{2+} and Ca^{2+}, and this sequence is consistent with the hydration energies of these cations.

Modeling High-pH Data

The predicted cation adsorption stayed constant above pH 6, but the experimental cation adsorption data continued to increase (Figs 1 and 2). Blank runs indicated significant precipitation above the pH range of the data shown in the

https://doi.org/10.1007/s42860-021-00115-y Published online by Cambridge University Press

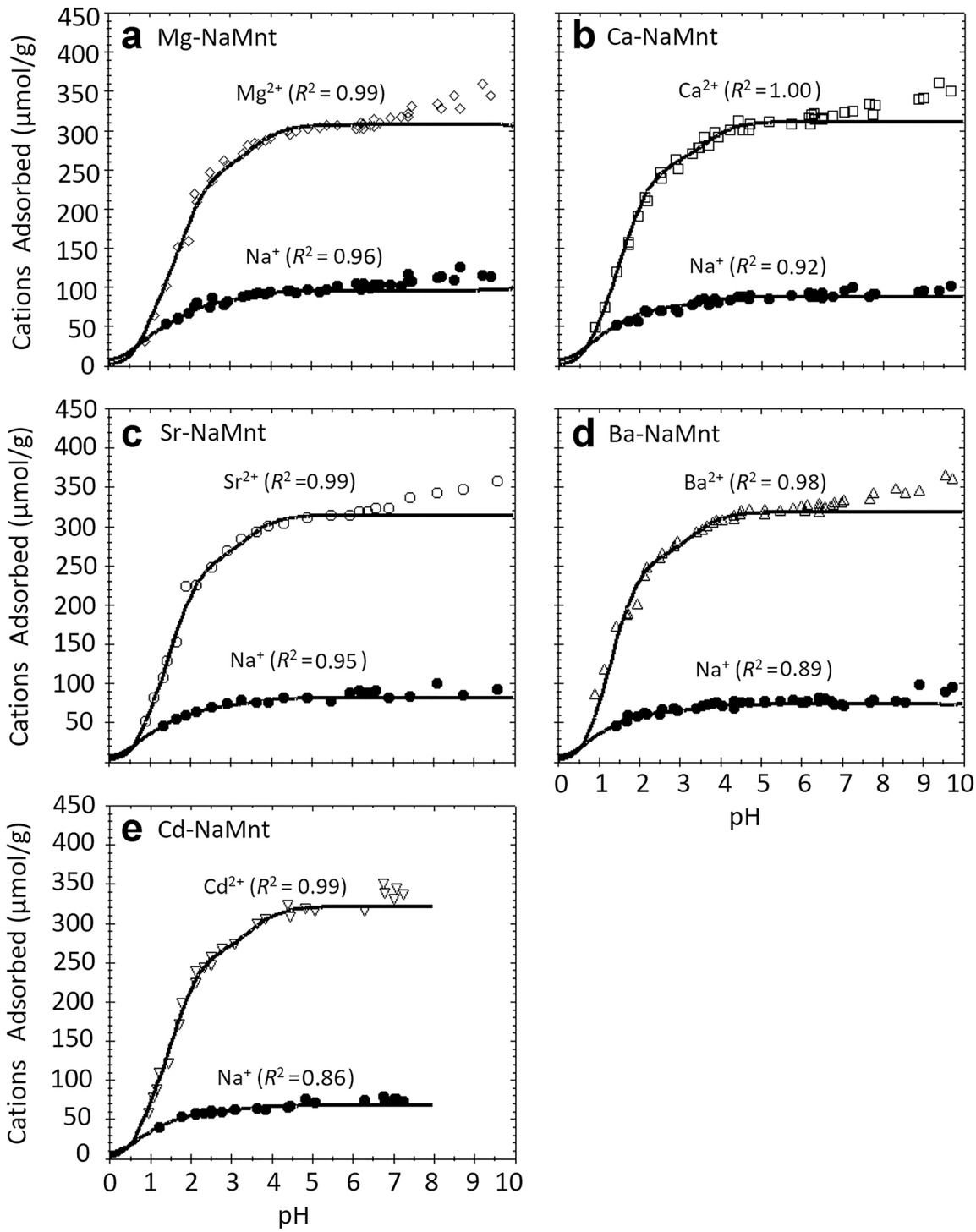


Fig. 2 Cation adsorption of **a** Mg^{2+}, **b** Ca^{2+}, **c** Sr^{2+}, **d** Ba^{2+}, or **e** Cd^{2+} on NaMnt as a function of pH. The initial conditions are shown in Table 2. Lines represent predicted adsorption data using the ion-exchange model. The CEC of each site and cation adsorption strength values are shown in Table 3a. The goodness-of-fit is Efron's pseudo-R^2 for pH < 6 data. The largest error was ±5.03 µmol/g for Na^+ and ±3.47 µmol/g for divalent cations

https://doi.org/10.1007/s42860-021-00115-y Published online by Cambridge University Press

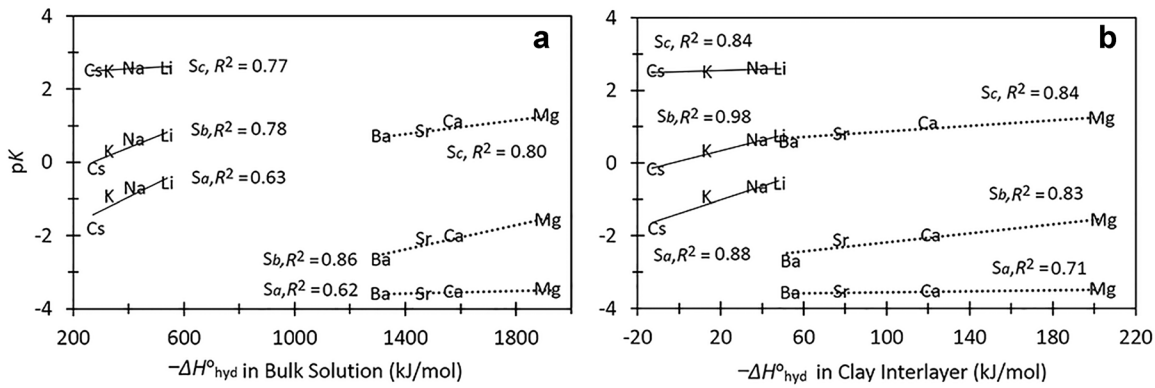


Fig. 3 The relation between negative logarithm of adsorption strength (p*K*) for monovalent alkali M^+ and divalent alkaline M^{2+} cations with their hydration energies ($-\Delta H^{o}_{hyd}$) in the **a** bulk solution and **b** clay interlayer. The p*K* values of monovalent alkali cations were from Li and Schulthess (2020). The hydration energy of cations in the bulk solution come from Smith (1977). The hydration energy of cations in the interlayer come from Salles et al. (2007, 2013)

figures, but very little precipitation of these cations in the pH range shown (<2.3% for Cd; <1.7% for Sr; <1.4% for Ba, Ca, and Mg). Adsorption modeling of cations at high pH generally includes metal hydroxide complexes in surface complexation reactions on the edge sites of clay minerals (Bradbury and Baeyens 2005; Fernandes and Baeyens 2019). These metal hydroxide complexation models indicate that the MOH^+ species exist at high pH and should be able to adsorb strongly, although Ferrage et al. (2005c) were unable to confirm the presence of these species using XRD profile modeling and near infrared spectroscopy. In the literature, the relative percentage of edge sites varied for different types of Mnt. Using potentiometric titration data curve fitting, the edge sites were estimated by Bradbury and Baeyens (2005) and Fernandes and Baeyens (2019) to be 8.6% of the total adsorption capacity of SWy-1 Mnt, by Missana and García-Gutiérrez (2007) to be 6% for FEBEX bentonite (Spain), and by Gu et al. (2010) to be 22.3% for Mnt (Upton, Wyoming, USA). Based on curve fitting of adsorption data and an assumed adsorption model, edge sites were estimated by Barbier et al. (2000) to account for 12.4% of total adsorption capacity for SWy-2 Mnt, and by Yu et al. (2015) for 5.6% for Mnt (Zhejiang, China). In general, the estimation of edge sites depends on curve fitting and their corresponding model assumptions. Accurate model fitting does not necessarily verify that the proposed model is correct and truthful. The near coincidence of the percentage of the edge sites on Mnt with the percentage of site S_c gives one pause to reconsider the proposed model assumptions.

Much smaller values for the edge sites are obtained with more direct measurement techniques. Using the Brunauer-Emmett-Teller method for external surface area and the ethylene glycol monoethyl ether method for total surface area analysis of SWy-1 Mnt clay, the edge sites were estimated by Schulthess and Huang (1990) to account for <3% of the total surface area. Using low-pressure gas adsorption and atomic force microscopy, the edge sites were estimated by Tournassat et al. (2003) to account for 1.1% of the total surface area of MX-80 Mnt. The measured edge site density was close to 10–15% from curve-fitting exercises after adjusting the measured value with a perimeter-to-area ratio of the clay according to Tournassat et al. (2003). Unclear, however, is whether this correction ratio is needed or whether the curve-fitted values are correct because that 14% of the adsorption site density can be modeled perfectly well without any contribution from the edge sites, as described below.

Some retention of cations on edge sites is likely, and its relative significance may be influenced by the particle size (Dzene et al. 2016). The tactoid size resulting from various interlayer cations is also believed to influence the relative retention of cations on external basal sites and interlayer sites (Tournassat et al. 2011). The particle size of SWy-1 smectite showed a bimodal distribution of diameters with

Table 4 Hydration energy and ionic radii of cations in this study

Cations	Hydration energy ($-\Delta H^{o}_{hyd}$, kJ/mol)		Ionic radius (Å)[d]
	In bulk water[a]	In clay interlayer	
H^+	1190	–	–
Na^+	410	38[b]	1.24
Mg^{2+}	1920	204[c]	0.80
Cd^{2+}	1810	–	1.00
Ca^{2+}	1560	120[c]	1.20
Sr^{2+}	1460	77[c]	1.30
Ba^{2+}	1320	52[c]	1.50

[a] Smith (1977), [b] Salles et al. (2007), [c] Salles et al. (2013), [d] Schulthess (2005)

https://doi.org/10.1007/s42860-021-00115-y Published online by Cambridge University Press

maxima at 300 and 1260 nm (Poli et al. 2008), and this size range suggests a significant role of the edge sites according to Dzene et al. (2016). When comparing two similar adsorption sites that reside in two environments, the adsorption strength will be much greater in the constrained environment than the non-constrained environment. This was illustrated with the retention of various cations in zeolite minerals of various pore sizes, and the phenomenon was described as the Nanopore Inner Sphere Enhancement (NISE) Effect (Schulthess et al. 2011). The Cs^+ cation was adsorbed more strongly in the interlayer sites of vermiculite than in the external (edge and basal) sites based on cation adsorption and desorption experiments (Dzene et al. 2016). Accordingly, the edge sites and external basal sites were not considered in the present study due to their lower CEC and weaker cation adsorption strength.

In the present study, the metal hydroxides (MOH^+) at high pH were proposed to adsorb on the clay interlayer sites via ion-exchange reactions rather than on the edge sites. Two pathways are possible for the retention of MOH^+: (1) the cations first hydrolyze in the liquid phase and then adsorb on the clay surface; or (2) the cations first adsorb on the clay surface and then hydrolyze while adsorbed.

For the first pathway, the sum of Eqs. 9 and 10 results in Eq. 11

$$M^{2+} + H_2O \rightleftharpoons MOH^+ + H^+ \tag{9}$$

$$S_iH + MOH^+ \rightleftharpoons S_iMOH + H^+ \tag{10}$$

$$S_iH + M^{2+} + H_2O \rightleftharpoons S_iMOH + 2H^+ \tag{11}$$

Under this pathway, the MOH^+ should be able to adsorb onto the strongest sites, namely S_a, followed by S_b, and lastly S_c. Significant formation of MOH^+ in the liquid phase did not occur until much higher pH values (~pH 11), which means that the presence of MOH^+ ions near the clay surface were too few and too short lived for their adsorption to occur at lower pH values (~pH 7).

For the second pathway, the sum of Eqs 12 and 13 results in the same Eq. 14:

$$2S_iH + M^{2+} \rightleftharpoons (S_i)_2M + 2H^+ \tag{12}$$

$$(S_i)_2M + H_2O \rightleftharpoons S_iMOH + S_iH \tag{13}$$

$$S_iH + M^{2+} + H_2O \rightleftharpoons S_iMOH + 2H^+ \tag{14}$$

Under this pathway, the hydrolysis of adsorbed M^{2+} on surface sites is favored at lower pH (~pH 7) because the change in the total Gibbs free energy for hydrolysis is favored when the mobility of the ions is reduced. That is, the mobility of the M^{2+} cation is reduced while adsorbed (Salles et al. 2013). This pathway is similar to pathways in surface catalysis. Reactions in surface catalysis are increased because: (1) concentrations of reagents increase in the surface phase; and (2) the activation energy barrier of one or more of the reagents is reduced because of the presence of the surface active sites (Fripiat and Van Damme 1983). The M^{2+} cation was strongly adsorbed onto sites S_a and S_b, and weakly adsorbed on site S_c (Table 3a). While significantly immobilized, the weaker adsorption of M^{2+} on S_c allows it to interact more easily and hydrolyze with the nearby H_2O molecules. Borrowing from gas-phase catalysis studies, the reactivity between species appears to be controlled primarily by adsorption energies (Montemore et al. 2017). For example, in Pt surface catalysis of O atoms with CO to form CO_2, the O atoms that were more reactive with the other substances present were those that were held loosely compared to the tightly held O atoms (Van Spronsen et al. 2017). Similarly, this proposed second pathway is preferred for S_c over S_b or S_a, and it is the assumed pathway in our model described below.

Equation 11 was added to the previous three-site ion-exchange model, where the equilibrium constants were defined as products over reactants:

$$K_{i,MOH} = \frac{\{S_iMOH\}(H^+)^2}{\{S_iH\}(M^{2+})} \tag{15}$$

The adsorption maximum (Γ_{max}) for each site was the same as Table 3, which equals the sum of adsorbed H^+, Na^+, and divalent cations:

$$\Gamma_{max,Si} = \{S_iH\} + \{S_iNa\} + 2\{(S_i)_2M\} + \{S_iMOH\} \tag{16}$$

All the model parameters were kept the same. The only unknown parameters were the K constants for Eq. 15, which were optimized based on the least squares of error using *IExFit* software. The optimization of the pK values showed that the three-site ion-exchange model was able to describe all the cation adsorption envelope data very well (Fig. 4). The model fit in Fig. 4 supported the hypothesis that adsorption occurred on sites S_c via the proposed second pathway, while a model based on the first pathway on sites S_a and S_b greatly overestimated the amount adsorbed at ~pH 7–8 (simulation not shown). Due to the lack of adsorption data at very high pH values, the pK values for the adsorption of MOH^+ on site S_a and S_b were estimated.

Using Ca^{2+} as an example, the surface cation speciation on Mnt is shown in Fig. 5. The Na^+ (S_iNa) adsorbed on sites S_a and S_b continued to increase with pH. On site S_c, S_cNa decreased at pH 6.5, and dropped to almost zero at ~pH 9. The amount of Na^+ adsorbed on three sites followed the order: $S_a > S_b > S_c$. The amount of divalent Ca^{2+} cation adsorbed increased with pH at low pH (<3), decreased slowly as pH increased, and finally, decreased rapidly at high pH (>9). The site S_a had a larger pH range for Ca^{2+} adsorption than S_b and S_c. When the monovalent $CaOH^+$ cation adsorbed increased at ~pH 11, 10, and 7 on sites S_a, S_b, and S_c, respectively, the amount of divalent Ca^{2+} cation adsorbed started to decrease. The $CaOH^+$ was predominantly adsorbed on site S_c when the pH was <10.

https://doi.org/10.1007/s42860-021-00115-y Published online by Cambridge University Press

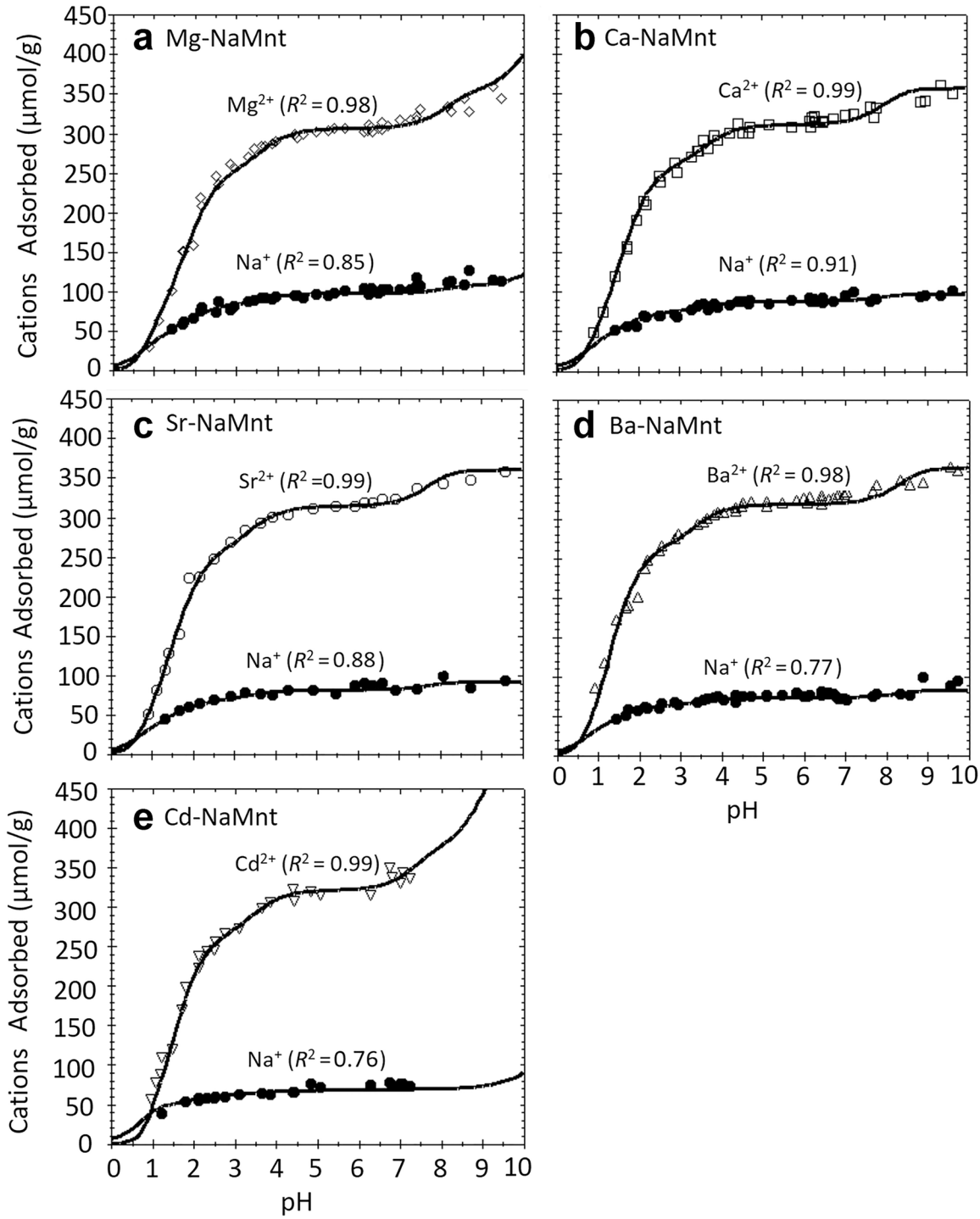


Fig. 4 Cation adsorption data of **a** Mg^{2+}, **b** Ca^{2+}, **c** Sr^{2+}, **d** Ba^{2+}, or **e** Cd^{2+} on NaMnt as a function of pH. The initial conditions are shown in Table 2. Lines are predicted adsorption data using the ion-exchange model and parameters are shown in Table 3. The goodness-of-fit is Efron's pseudo-R^2

Implication and Confirmation of the Ion-Exchange Model

Note that this new approach of describing adsorption data at high pH also predicted an increase in Na^+ retention at ~pH 9 (Figs 4 and 5). Published Na^+ adsorption envelope data typically show increased Na^+ adsorption at high pH (Nolin, 1997; Motellier et al. 2003; Jacquier et al. 2004).

https://doi.org/10.1007/s42860-021-00115-y Published online by Cambridge University Press

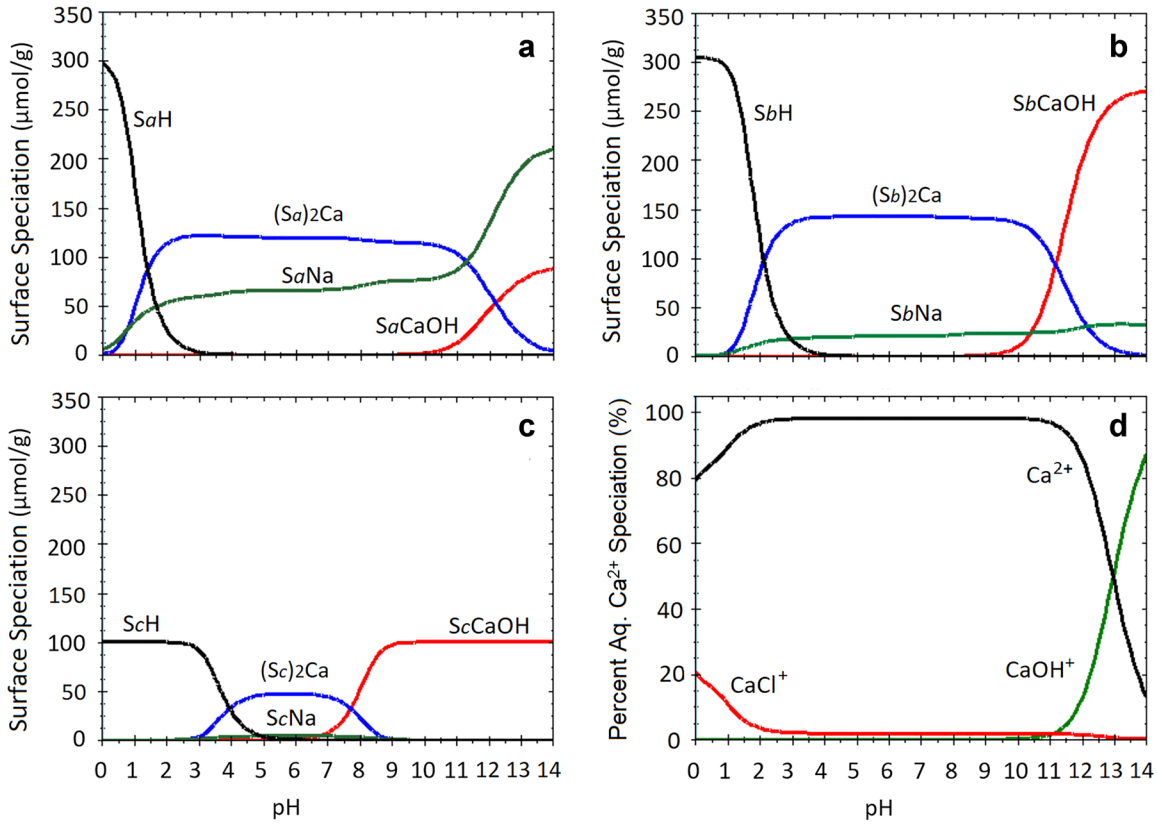


Fig. 5 Model simulation of surface cation speciation on sites **a** S_a, **b** S_b, and **c** S_c on NaMnt, and **d** Ca^{2+} aqueous speciation on NaMnt from Fig. 4b

Whereas models can be proposed that describe the retention of Na^+ cations at high pH using new adsorption sites, the alternative model proposed here suggested the retention of Na^+ cations on existing interlayer sites with hydrolyzed divalent cations. The predicted increase in Na^+ adsorption at pH 8–10 is due to the retention of $CaOH^+$ species on site S_c, which resulted in a net reduction of Ca^{2+} competition on Na^+ adsorption. Very few published articles have explored the inclusion of $CaOH^+$ in their models as a viable adsorbing species, and they generally involve both interlayer and edge sites. A surface complexation model involving an ion-exchange reaction between $SrOH^+$ and H^+ to predict the cation adsorption data on MX-80 Wyoming bentonite was developed by Molera et al. (2002). The ion-exchange reaction between $CaOH^+$ and Na^+ in two different types of models were used by Tournassat et al. (2004a) to predict the cation adsorption data on the MX-80 Mnt. The model proposed in Table 3 here is a significant alternative to the introduction of a new adsorption edge site.

When there was no Ca^{2+} present, the predicted Na^+ adsorption remained almost constant at high pH (Fig. 6), which was confirmed by Li and Schulthess (2020). With 0.5 mmol/L Ca^{2+} added, the predicted Na^+ adsorption curve showed a new edge at ~pH 10 (labeled 'A' in Fig. 6). With 1 mmol/L Ca^{2+} added, another new adsorption edge appeared at ~pH 13 (labeled 'B'). As the Ca^{2+} concentration increased, the two new adsorption edges shifted to lower pH ranges, and were most prominent at Ca^{2+} concentrations of 1–2 mmol/L for these initial Na^+ concentrations. The

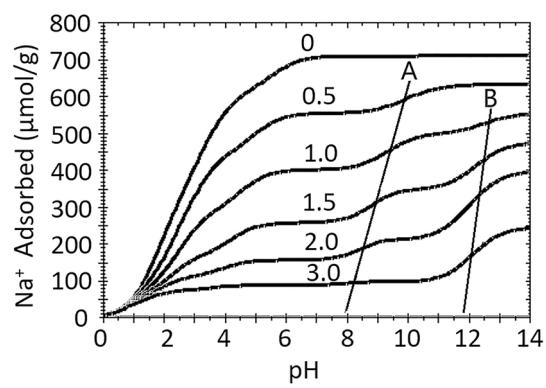


Fig. 6 Predicted Na^+ adsorption on Mnt with various levels of Ca impurities (mmol/L) using the ion-exchange model and model parameters shown in Table 3. The total Na^+ was 5.44 mmol/L, and the clay concentration was 6.46 g/L. Lines A and B show the positions of the new adsorption edges on the Na^+ adsorption curves

https://doi.org/10.1007/s42860-021-00115-y Published online by Cambridge University Press

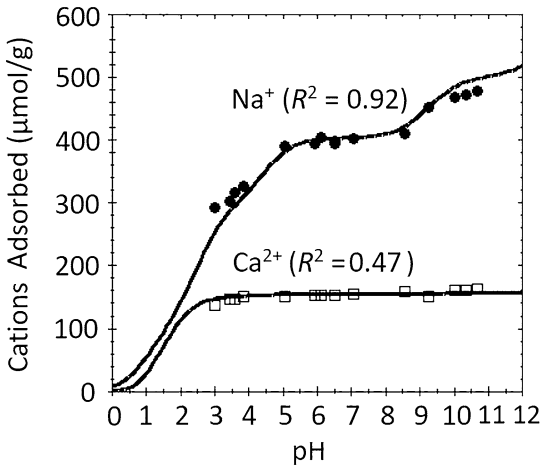


Fig. 7 Predicted Ca^{2+} and Na^{+} adsorption on Mnt using ion-exchange model. Model parameters are shown in Table 3. The total Ca^{2+} and Na^{+} were 1.00 and 6.44 mmol/L, respectively. The clay concentration was 6.46 g/L. The largest error was ±5.98 μmol/g for Na^{+} and ±1.32 μmol/g for Ca^{2+}

predicted increase in Na^{+} retention at high pH almost disappeared when the Ca^{2+} concentration reached 3 mmol/L (Fig. 6), confirmed in Fig. 4b.

In order to examine better the influence of Ca^{2+} on Na^{+} adsorption using this model, a cation adsorption experiment on NaMnt was conducted as a function of pH with 1 mmol/L Ca^{2+} added (Fig. 7). The ion-exchange model and model parameters in Table 3 predicted the Na^{+} and Ca^{2+} adsorption very well. A new edge appeared at ~pH 9 in the Na^{+} adsorption curve which was not readily apparent at higher Ca^{2+} concentrations or in the absence of Ca^{2+} cations, but was consistent with the predictions in Fig. 6.

Whereas site S_c plays a significant role in the retention of MOH^{+} cations (Figs 5 and 6), no clear proof of the role of sites S_a and S_b was shown in the present study. The estimated pK values of $CaOH^{+}$ adsorption on sites S_a and S_b were 10 (Table 3b), but these values were quite arbitrary. A reasonable assumption is that if aqueous $CaOH^{+}$ is naturally present at high pH values (Fig. 5d), then a strong possibility exists that this species will remain stable long enough to react with sites S_a and S_b. That is, the reaction would follow pathway 1 described above with Eqs. 9 and 10. Accordingly, setting the pK values to 10 for the $CaOH^{+}$ adsorption on sites S_a and S_b resulted in the formation of S_aCaOH and S_bCaOH species at nearly the same pH range (Fig. 5a, b) as the formation of $CaOH^{+}$ species in the liquid phase (Fig. 5d). Similar reasoning was applied for estimating the pK values of the other divalent cations on sites S_a and S_b.

In the pH-dependent Na^{+} adsorption data as a function of Ca^{2+} concentrations, a 4- or 5-site model (including interlayer sites and edge site) could be proposed easily based on the multiple adsorption edges in the adsorption envelope curves (Fig. 7). This confirmed that the model assumptions can have many consequences for understanding how and why the clay behaves the way it does. Traditionally, proposed models have been supported predominantly by curve-fitting adsorption data, where the number of sites is based on the number of edges in adsorption envelopes or the number of linear regression curves of adsorption isotherms (Nolin 1997; Motellier et al. 2003; Missana et al. 2014; Robin et al. 2015). The present study, however, showed that new edges in the adsorption envelope curve do not necessarily correspond to reactions on new adsorption sites on the clay surface. Instead, the new edges indicate possible new reactions on the existing adsorption sites. Specifically, the adsorption of metal hydroxide does not necessarily need to be on the clay's edge sites, but instead could be a competitive ion-exchange reaction on the interlayer sites.

In the current study, the number of adsorption sites and relative percentage of each site were based on probabilities of the distances between octahedral Fe^{3+} and Mg^{2+} cations in a presumed Mnt with chemical formula $H[Al_6MgFe]Si_{16}O_{40}(OH)_8$, the composition of which is similar to the natural SWy-3 Mnt (Li et al. 2020). These pre-determined parameters help increase the certainty of ion-exchange models. The identification of a number of adsorption sites using DFT simulations can be applied potentially to other 2:1 expansive clay minerals. For example, if the ratio of octahedral Al^{3+} decreases and the Fe^{3+}:Mg^{2+} ratio increases, the percentage of octahedral Fe^{3+} and Mg^{2+} with shorter distance will increase, the number of sites with weaker adsorption strength (i.e. S_c) will decrease, and the number of sites with stronger adsorption strength (i.e. S_a and S_b) will increase. Other substitutions in the clay structure (such as Ti^{4+} or Mn^{2+}, or tetrahedral substitutions) will also influence the proportion of adsorption sites and resultant cation adsorption strength.

Relationship Between Interlayer Spacing and pK Values

The interlayer cations were retained on Mnt clay surfaces with variable adsorption strength (Table 3). Accordingly, the interlayer cation composition on Mnt changed as a function of pH and total cation concentrations (Fig. 4). The interlayer cation species also impact the interlayer spacing of SWy-1 samples under controlled relative humidity (Ferrage et al. 2005a, 2005c) and water-saturated Wyoming Mnt samples (Norrish and Quirk 1954). Thus, the interlayer spacing of Mnt was analyzed to investigate its relationship with the cation adsorption strength.

A key feature of the model proposed in the current study is the constant pK values for the Na^{+} cation in the presence of various competing cations. This is justified if ion–ion interactions among different types of cations in the interlayer space are minimal. One way to minimize these effects in the interlayer sites is to segregate the adsorbed cations. Using XRD analysis and adsorption isotherm data of Ca-NaMnt (Camp-Berteaux, France), the concept of 'demixing' was proposed by Glaeser and Méring (1954), where some interlayer spaces are occupied

https://doi.org/10.1007/s42860-021-00115-y Published online by Cambridge University Press

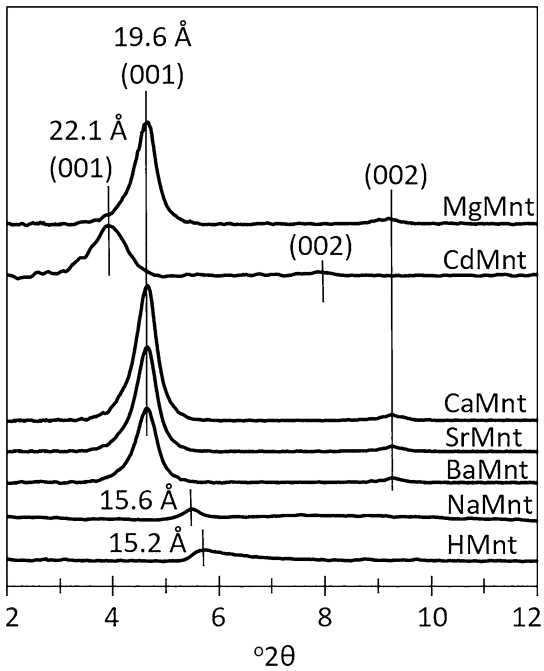


Fig. 8 XRD patterns of wet Mnt saturated with Mg^{2+} (MgMnt), Cd^{2+} (CdMnt), Ca^{2+} (CaMnt), Sr^{2+} (SrMnt), Ba^{2+} (BaMnt), and Na^{+} (NaMnt) cations at ~pH 7, and H^{+} (HMnt) cation at pH < 1. The d_{001} values (Å) are also shown

mainly by Ca^{2+} ions and others mainly by Na^{+}. Two distinct XRD peaks from bi-ionic Na-Ca Mnt samples (Clay Spur, Wyoming, USA) were observed by Levy and Francis (1975) when the adsorbed Na^{+} was 40% and 60%, and those authors suggested that segregation of cations in different layers occurred. After treating a bi-ionic K-Ca Mnt (Camp-Berteaux, France) with alternating wetting and drying cycles, a progressive separation of two phases was observed by Mamy and Gaultier (1979): an organized phase saturated with K^{+} cations, and a disorganized phase containing K^{+}-Ca^{2+} mixtures. After comparing measured and calculated XRD patterns of 11 different types of dioctahedral smectites and two interstratified mica/smectite clays containing various ratios of Ca^{2+} and Na^{+} cations (Japan), the Na^{+} and Ca^{2+} cations tend to segregate and form Ca-dominant and Na-dominant interlayer structures according to Iwasaki and Watanabe (1988). The demixing of Ca^{2+} and monovalent ions (Na^{+}, K^{+}, NH_4^{+}) on smectite colloids (extracted from Zook soil, Story County, Iowa, USA) was also suggested by Pils et al. (2007), based on observed shifts and the presence of multiple XRD peaks. The segregation of ions observed in the present studies suggested that ion–ion interactions are minimal among different types of ions inside the interlayers. This is consistent with Pauling's rule #5, where the number of different kinds of constituents in a crystal environment tends to be small. This also supports the use of constant p*K* values in the proposed adsorption model discussed earlier.

X-ray diffraction patterns of the centrifuged Mnt samples from cation adsorption envelopes were analyzed to explore whether the present clay samples also showed signs of cation segregation. The clay samples were analyzed immediately after centrifugation to ensure *in situ* hydration of the interlayer cations. The water contents of all samples were within a range of 70–78% (equivalent to 2.33–3.55 g of water per g of dry clay sample), which resulted in a variability of 0.2 Å in d_{001} values. Note that water retention by clay samples is sensitive to centrifugation speeds (Fehervari et al. 2019). Accordingly, the XRD results in the present study are specific to the centrifuge treatments applied.

The Mnt saturated with alkaline earth cations had the same d_{001} value of 19.6 Å (Fig. 8). The Mnt saturated with Cd^{2+}, Na^{+}, and H^{+} showed d_{001} values of 22.1, 15.6, and 15.2 Å, respectively. The relative intensity of the d_{001} peaks in the XRD patterns of Mnt saturated with divalent cations was ~7 times greater than that of NaMnt and HMnt, and this may be because the NaMnt and HMnt particles do not stack as well as the Mnt saturated with divalent cations. The decrease in the XRD intensities as a function of decrease in clay particle stackings was reported in the literature. The stability of soil smectite colloids by mixing clay-humic complexes (Zook soil from the surface 0–40 cm of a pedon in Story County, Iowa, USA) with various ratios of monovalent cations (Na^{+}, K^{+}, NH_4^{+}) to Ca^{2+} was suggested by Pils et al. (2007), who further suggested that the broadening and decrease in the intensity of XRD patterns were consistent with the breakup of large quasicrystals to medium and small quasicrystals and the increased dispersion of quasicrystals. Decreases in XRD peak intensities when SWy-2 Mnt was acid-activated with 0.25 M H_2SO_4 was observed by Bhattacharyya and Gupta (2008) who suggested that the decrease in XRD peak intensity implied the dispersion and amorphization of the acid-treated clay compared to the original one. The effect of wet grinding on the mesoporous properties of Mnt (Jilin, China) was studied by Xia et al. (2010) who attributed the decrease in XRD d_{001} peak intensities to the disrupted and lost stacking of clay layers due to the wet grinding. Decreases in the XRD d_{001} peak intensities of Mnt (Zhejiang, China) after several cycles of freezing/thawing-ultrasonic exfoliation process were observed by Chen et al. (2019) who suggested that the degree of order of the lamellar structure of Mnt decreased.

The d_{001} values of 15.6 Å for NaMnt are similar to the values in the literature, e.g. a value of 15.2 Å when the Na-saturated SWy-1 Mnt was water-saturated was noted by Chiou and Rutherford (1997). A value of 15.6 Å was observed by Oueslati et al. (2012) for Na-saturated SWy-2 Mnt at 95% RH after 5 or 10 cycles of hydration–dehydration. The d_{001} values of 15.6 Å for NaMnt (Fig. 8) were also similar to the values obtained by Li and Schulthess (2020) for water-saturated HMnt (15.2 Å) and LiMnt (15.9 Å), but greater than the values for KMnt (13.6 Å) and CsMnt (12.5 Å). Larger d_{001} values for Na-saturated Mnt are also to be found in the literature. A value of 18.73 Å was obtained by Dazas et al. (2014) for Na-saturated SWy-2 Mnt at 98% RH. d_{001} values of between

https://doi.org/10.1007/s42860-021-00115-y Published online by Cambridge University Press

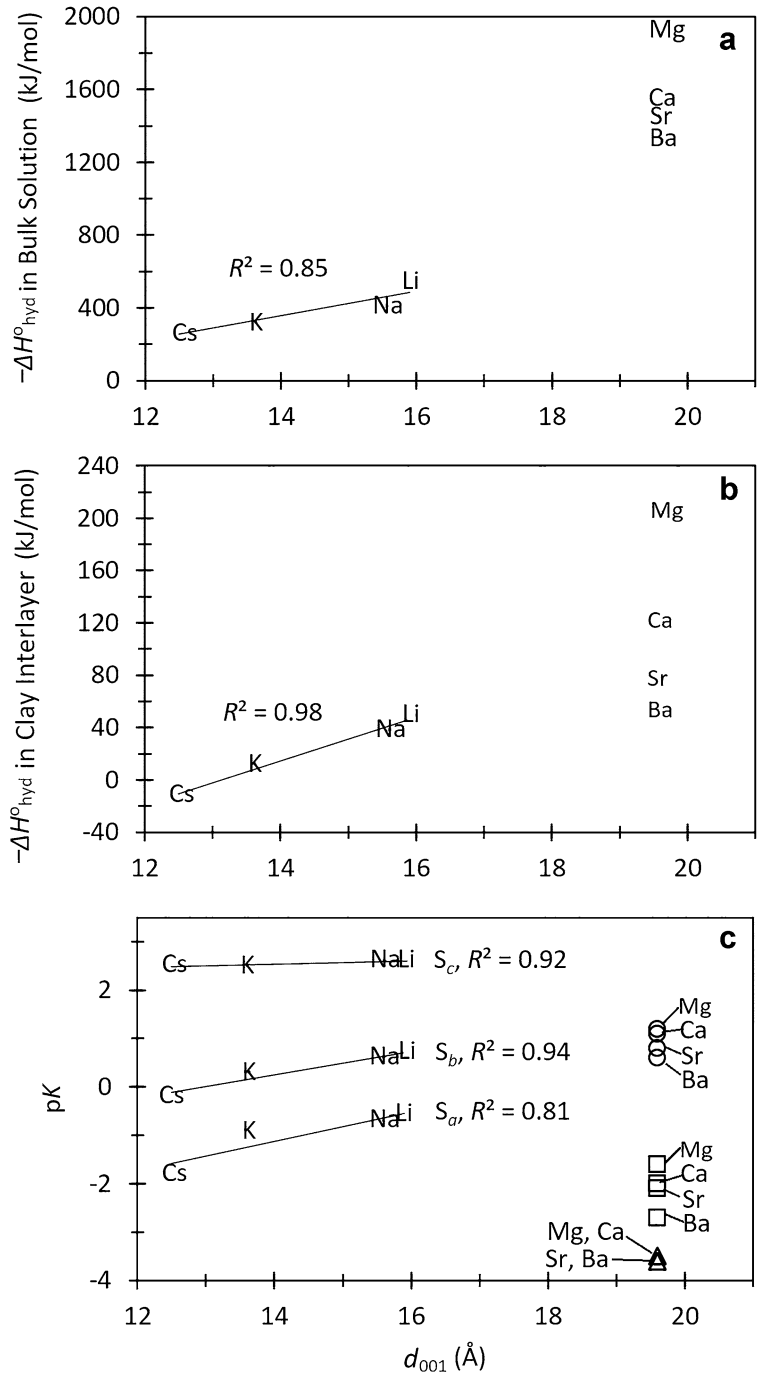


Fig. 9 The relation of d_{001} values of cation-saturated Mnt with hydration energies ($-\Delta H^{o}_{hyd}$) of monovalent alkali M^{+} and divalent alkaline earth M^{2+} cations in **a** bulk solution and **b** clay interlayer, and **c** their negative logarithm of adsorption strength (pK). The pK values of monovalent alkali cations were from Li and Schulthess (2020). The position of the letters without symbols indicates the location of the data points for corresponding elements

17.51 and 18.72 Å were observed by Oueslati et al. (2017) for the Na-saturated SWy-2 Mnt at 90% RH. The difference in d_{001} values of Na-saturated Mnt may be due to the sample pretreatments (e.g. methods to control sample water content, centrifugation). The larger d_{001} values of ~19.6 Å for divalent cation-saturated Mnt are also similar to reported values in the

https://doi.org/10.1007/s42860-021-00115-y Published online by Cambridge University Press

Table 5 Number of interlayer water layers for various d_{001} values (Å) of Wyoming Mnt used in XRD profile modeling in the literature

Cation	Number of water layers					Reference
	0W	1W	2W	3W	4W	
Li, Na, K, Mg, Ca, Sr	9.6–10.0	11.5–13.0	13.9–15.8	18.0–18.5		Ferrage et al. (2005a)
Li, Na, K, Rb, Cs, Mg, Ca, Sr, Ba	10.0	12.5	15.0	17.5	20.0	Laird (2006)
Li, K, Rb, Cs, Mg, Sr, Ba, La	9.8	12.1–12.5	14.6–16.2			Morodome and Kawamura (2011)
Cd		12.4	15.4	18.1		Oueslati et al. (2011)
Na, Ca	9.2–10.1	12.2–12.7	15.2–15.7	18.4–19	21.4–22	Holmboe et al. (2012)
Na, Mg, Ca, Ba	9.6–10.2	11.6–12.9	14.9–15.7	18–19		Dazas et al. (2014)
Li, Na, K, Cs		12.5	15.6			Li and Schulthess (2020)
H			15.2			Present study
Mg, Ca, Sr, Ba				19.6	20.3, 22.1	
Cd					22.1	
$MgCl^+$, $CaCl^+$, $SrCl^+$, $BaCl^+$, $CdCl^+$			22.1			

literature. Values of 19.23, 18.93, and 18.90 Å were observed by Dazas et al. (2014) for Mg-, Ca-, and Ba-saturated SWy-2 Mnt at 98% RH.

The Mnt saturated with monovalent alkali cations showed a strong linear correlation between d_{001} and pK values, and between d_{001} and hydration energy (Fig. 9). However, the d_{001} values of Mnt saturated with different divalent alkaline earth cations remained the same regardless of the hydration energy and pK values of these cations. Similar efforts have been made to correlate d_{001} values with the cation's ionic potential (valence/radius ratio) (Dazas et al. 2014), where the ionic potential was related to hydration energies (Smith 1977). A good correlation was observed by Dazas et al. (2014) of the ionic potential with layer-cation mean distance using profile modeling of 001 reflections of 3-hydrated SWy Mnt at 98% RH based on observed d_{001} values of Mg-SWy (19.23 Å), Ca-SWy (18.93 Å), and Ba-SWy (18.90 Å). The lack of any correlations observed for divalent ions in Fig. 9 suggested that these correlations are observed easily with weakly held monovalent cations, but not with strongly held divalent cations. The correlations observed in Fig. 3 for both monovalent and divalent cations support strongly the relation between hydration energies and retention strength. The relation of retention strength and hydration energies to interlayer dimensions was not substantiated with divalent cations in the current study, however (Fig. 9). The same d_{001} values of Mnt saturated with various divalent alkaline earth cations may be due to the strong hydration energy of these cations (Fig. 9a,b), which stabilized more water molecules in the interlayer sites and kept a constant d_{001} value for the clay.

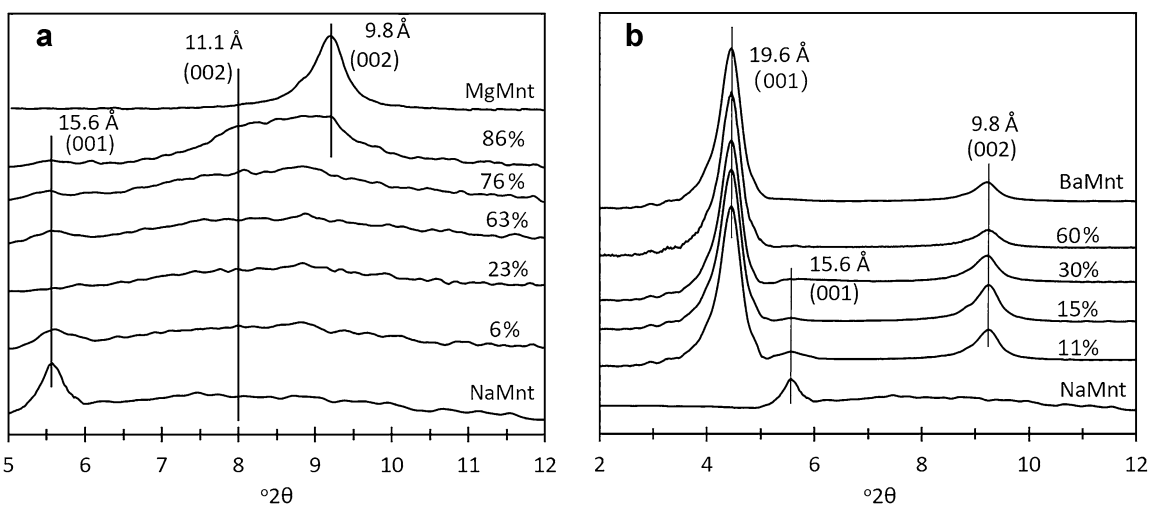


Fig. 10 XRD pattern of wet NaMnt with various equivalent fractions of adsorbed **a** Mg^{2+} at pH 7.5 and **b** Ba^{2+} at pH 8. The d_{001} reflections of the peaks for 22.1 and 19.6 Å are at 4.0 and 4.6°2θ, respectively, as noted in Fig. 8

https://doi.org/10.1007/s42860-021-00115-y Published online by Cambridge University Press

That is, although variations in the hydration energy did correlate well with the p*K* values (Fig. 3), the weakest hydration energy of divalent cations (namely, Ba^{2+}) was still too strong to collapse the interlayer space. Consequently, no d_{001}-p*K* or d_{001}-hydration energy correlations were observed with divalent cations.

The layers of water molecules surrounding interlayer cations was calculated roughly by dividing the interlayer hydration thickness by the diameter of water molecules (2.74 Å; Schatzberg 1967). The hydration thickness was obtained by subtracting the layer thickness (9.6 Å; Schoonheydt et al. 2011) and diameter of interlayer cations (Table 4) from the measured d_{001} values. Accordingly, the calculated layers of water molecules correspond to 3W or 4W for alkaline earth cations, 4W for Cd^{2+}, 2W for Na^{+}, and 2W for H^{+}. These numbers agreed with the general values reported in XRD profile modeling in the literature for the degree of hydration as a function of measured d_{001} values (Table 5). Note that the interlayer divalent cations had more interlayer water (2–4 layers of water) than the interlayer monovalent cations in Mnt (1–2 layers of water). Whether the interlayer divalent cations were inner sphere adsorbed or outer sphere adsorbed is unclear, but they did, at least, stabilize the presence of water molecules in the interlayer much more than the monovalent cations. This is consistent with the stronger hydration energy of divalent cations relative to monovalent cations.

The Mnt saturated with various cations had different interlayer spacing (Fig. 8). These homoionic clay samples were end members of a progressive mixing of competitive cations. The XRD pattern of Mnt samples can reveal if these mixed cation ratios exist as mixed or segregated species in the clay interlayers. Accordingly, the Mnt samples with various percentages of adsorbed Mg^{2+} and Na^{+} were analyzed with XRD (Fig. 10a). The percentages of adsorbed Mg^{2+} and Na^{+} on Mnt were predicted using the ion-exchange model and parameters proposed in this study (Table 3). Note that the XRD patterns shown in Fig. 10a started at 5°2θ, and thus captured only the weaker d_{002} peaks. The peak corresponding to 15.6 Å in the XRD patterns became smaller when the equivalent fractions of adsorbed Mg^{2+} was 6% of the total CEC, still existed when the equivalent fractions of adsorbed Mg^{2+} was 86% of the total CEC, and disappeared when the clay was saturated with Mg^{2+}. A broad d_{002} peak at 8.0°2θ corresponding to 22.1 Å appeared gradually and was discernible when the equivalent fraction of adsorbed Mg^{2+} was 86% of the total CEC. This 22.1 Å peak was also observed at low pH conditions (see Fig. 11), and tentatively may be the result of an intermediate interstratification structure. It might also be due to $MgCl^{+}$ retention in the interlayer. The presence of metal-Cl^{+} ion pairs in the interlayer of SWy-2 Mnt clays was also noted by Ferrage et al. (2005b). At 86% MgMnt retention, $MgCl^{+}$ accounted for ~1.7% of the total Mg species in solution.

Conversely, the XRD pattern of Mnt samples with various percentages of adsorbed Ba^{2+} did not show a peak at 22.1 Å. This XRD set only reached a maximum of 60% BaMnt, with ~0.2% as $BaCl^{+}$ of the total Ba species in solution. The BaMnt characteristic d_{001} peak at 4.5°2θ and d_{002} peak at 9.0°2θ corresponding to 19.6 Å appeared when the equivalent fraction of adsorbed Ba^{2+} was >11% of the total CEC, which suggested the formation of interlayers dominated with Ba^{2+} cations. The XRD peak of NaMnt at 15.6 Å became significantly smaller when the equivalent fraction of adsorbed Ba^{2+} was 11% of the total CEC, and disappeared when the fraction of adsorbed Ba^{2+} was >60%, which suggested that the interlayer Na^{+} was gradually replaced by the Ba^{2+} cations.

The adsorbed cations on Mnt increased with pH (Figs. 4 and 5). The corresponding relative percentage of adsorbed interlayer cations also increased with pH (Fig. 11). The d_{001} of Mnt adsorbed with alkaline earth cations (Mg^{2+}, Ca^{2+}, Sr^{2+}, and Ba^{2+}) decreased from 22.1 to 20.3 and 19.6 Å when pH increased (Fig. 11), which suggested that the interlayer alkaline earth cations on Mnt were predominantly hydrated with four layers of water at low pH, but changed gradually to predominantly three layers of water (Table 5). The Mnt adsorbed with Cd^{2+} kept constant at 22.1 Å, which suggested that the Cd^{2+} on Mnt were predominantly hydrated with four layers of water regardless of the pH. Alternatively, the number of water layers is reduced to 2W for d_{001} peaks at 22.1 Å if the interlayer cations are MCl^{+} species, which, from aqueous speciation calculations, are particularly likely to occur with $CdCl^{+}$ at pH < 10 and with the alkaline earth cations at pH < 2. Unlike the alkaline earth cations, the Cd^{2+} cations can form strong $CdCl^{+}$ complexes over a wide pH range.

Most of the broad peaks around 4°2θ in Fig. 11 appear to be the result of several overlaid peaks, corresponding to 22.1, 20.3, and 19.6 Å. The presence of multiple d_{001} peaks for Mnt samples with various percentages of interlayer cations (Figs. 10 and 11) suggested the formation of different interlayers containing dominantly one type of cation, which were described as segregated layers or a demixing process by Glaeser and Méring (1954), Levy and Francis (1975), Mamy and Gaultier (1979), Iwasaki and Watanabe (1988), and Pils et al. (2007).

An alternative explanation for the presence of multiple peaks can be the heterogeneity of the interlayer hydration state of clay minerals. The shift and presence of coexisting XRD peaks on Ca-saturated SWy-2 Mnt from 15.2 Å at near-neutral pH to 12.6 Å at pH 0.14 were observed by Ferrage et al. (2005c) who suggested a modification of the smectite interlayer composition in the presence of interlayer protons at low pH. Extremely heterogeneous structures including interstratification of 2W and 1W at intermediate pH were also observed in their study. The shift and presence of coexisting XRD d_{001} peaks from a mainly monohydrated structure for the Na-saturated SWy-2 Mnt to a bihydrated structure for the Ca-saturated Mnt as a function of the equivalent fractions of Na^{+} in solution were observed by Tertre et al. (2011) and noted to adsorb on the solid. Those authors suggested that this change in XRD peaks resulted from a modification of the Mnt hydration state. A

https://doi.org/10.1007/s42860-021-00115-y Published online by Cambridge University Press

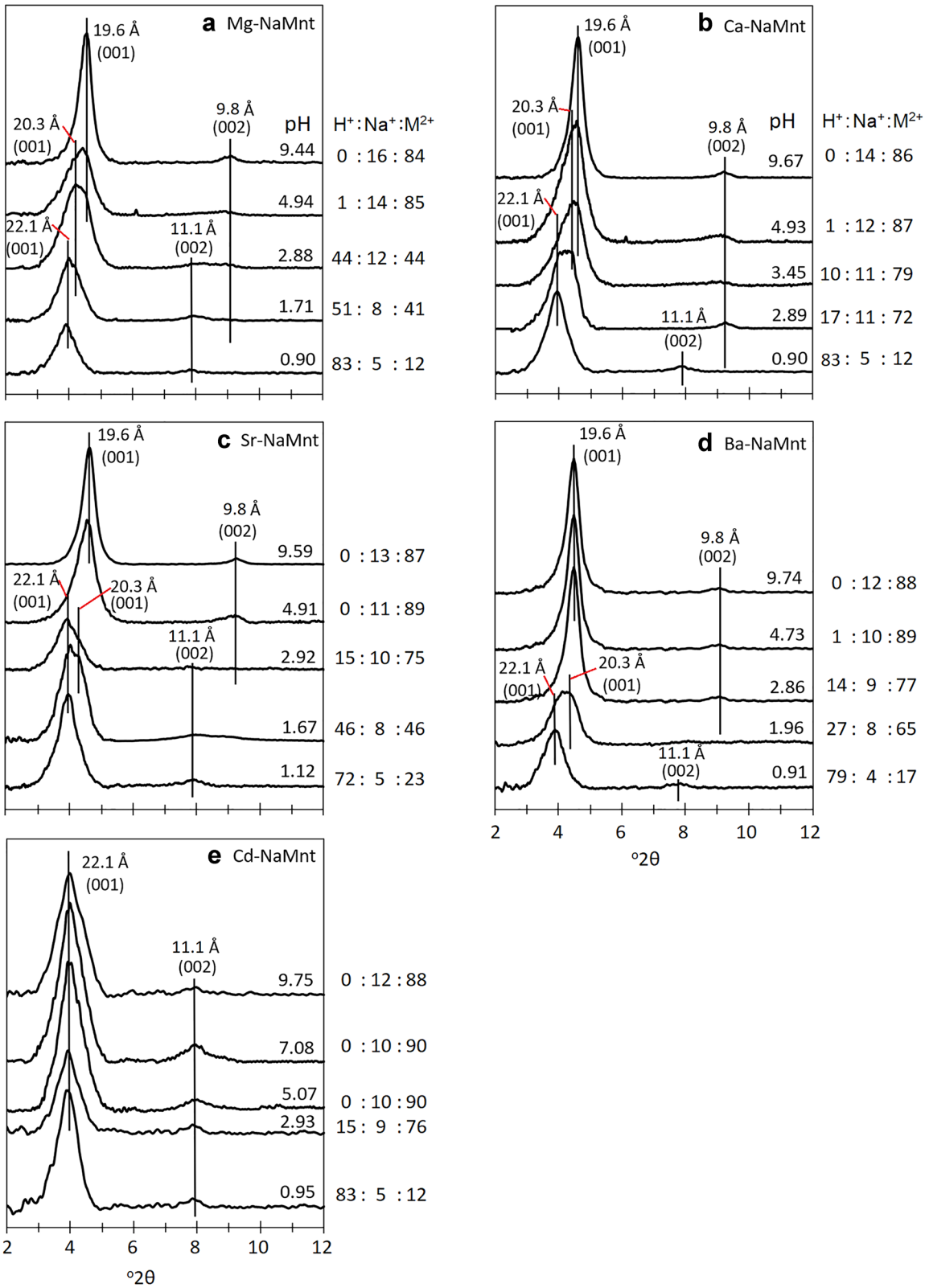


Fig. 11 XRD patterns of wet Mnt samples from **a** Mg^{2+}, **b** Ca^{2+}, **c** Sr^{2+}, **d** Ba^{2+}, and **e** Cd^{2+} adsorption envelopes at various pH values. The d_{001} values (Å) and the model predicted ratios of adsorption sites occupied by different cations are also shown

https://doi.org/10.1007/s42860-021-00115-y Published online by Cambridge University Press

third possible explanation is the presence of impurities (e.g. feldspar, illite, quartz) in NaMnt samples. Thirty six bentonite samples were studied by Kaufhold et al. (2011) who observed that the presence of impurities changed the XRD peak shape and position.

The XRD peak at 22.1 Å was observed in all samples at low pH and in Cd-NaMnt at all pH values (Fig. 11). This may be due to the formation of intermediate interlayer structures or the presence of other ions in the interlayer, resulting in modification of the interlayer dimensions, potentially $M\text{Cl}^+$ cations. The estimated aqueous $M\text{Cl}^+$ percentages of total alkaline earth metal concentrations in solution were ~1% or higher for all samples that showed an XRD peak at 22.1 Å. The estimated percentages of aqueous CdCl^+ of the total Cd in solution ranged from 27% at high pH to 63% at low pH.

CONCLUSIONS

The adsorption of divalent cations was described very well using an extension of an ion-exchange model developed for monovalent cations. Confidence in the model is enhanced when some of its parameters are obtained independently. Specifically, the number of adsorption sites and relative percentage of CEC for each site were taken from a previous DFT study (Li et al. 2020).

At low pH (< 6), an ion-exchange model involving H^+, Na^+, and M^{2+} described the cation adsorption envelope data very well. The adsorption strength of divalent cations increased in the order $Mg^{2+} < Cd^{2+} < Ca^{2+} < Sr^{2+} < Ba^{2+}$ on all three sites, which was in the opposite order of their hydration energies.

At higher pH (> 6), the cation adsorption continued to increase with pH. Accordingly, the metal hydroxide species, $M\text{OH}^+$, was added to the previous ion-exchange model and the new model was able to describe cation adsorptions very well on NaMnt. Although the aqueous $M\text{OH}^+$ started to form at ~pH 10, the adsorption of $M\text{OH}^+$ at ~pH 7 on site S_c suggested that M^{2+} was first adsorbed on the clay surface and then hydrolyzed while adsorbed.

The presence of M^{2+} cations resulted in the formation of new adsorption edges in the Na^+ adsorption envelope curve. The present study showed that these new adsorption edges are not necessarily adsorption reactions on new adsorption sites, but could instead be new adsorption reactions on the existing sites. To be clear, adsorption on clay edges can exist, but their contribution to the total CEC of the SWy-3 Mnt is probably much lower than traditionally asserted; possibly as low as 1% of the total CEC, consistent with their surface area and site density contribution for MX-80 (Tournassat et al. 2003) or 3% for SWy-1 (Schulthess and Huang 1990).

The d_{001} values of Mnt can be influenced by sample pretreatments. The Mnt saturated with divalent cations showed larger d_{001} values than monovalent cations, as expected, because the divalent cations have stronger hydration energies (Morodome and Kawamura 2011). The Mnt showed a consistent d_{001} value of 19.6 Å when saturated with alkaline earth cations (Mg^{2+}, Ca^{2+}, Sr^{2+}, Ba^{2+}), and 22.1 Å with Cd^{2+}. The interlayer divalent cations were hydrated with 3 or 4 water layers, whereas interlayer monovalent cations were hydrated with 1 or 2 water layers. The amount of interlayer water was consistent with their hydration energies. Unlike monovalent cations, no relation was found between the measured d_{001} values and the negative logarithm of adsorption strength for divalent cations. The presence of multiple d_{001} peaks in the XRD patterns suggested that the interlayer cations were segregated and that the interlayer ion–ion interactions among various types of ions were minimized. Minimizing ion–ion interactions among various types of ions in the interlayer is an important criterion for maintaining a constant pK value for Na^+ in the ion-exchange model of mixed-cation systems.

ACKNOWLEDGMENTS

The authors acknowledge the assistance of Dawn Pettinelli, Joseph Croze, and Patrick McIntosh of the University of Connecticut Soil & Nutrient Analysis Laboratory. They also thank the journal reviewers for their constructive comments. This work was supported by the USDA National Institute of Food and Agriculture, Hatch project accession number 1013470. Funding support also came from the 2018 Student Research Grant Award from The Clay Minerals Society.

Funding

Funding sources are as stated in the Acknowledgments.

Declarations

Conflict of Interest

The authors declare that they have no conflict of interest.

REFERENCES

Bala, P., Samantaray, B. K., & Srivastava, S. K. (2000). Dehydration transformation in Ca-montmorillonite. *Bulletin of Materials Science, 23*, 61–67.

Baeyens, B., & Bradbury, M. H. (1997). A mechanistic description of Ni and Zn sorption on Na-montmorillonite Part I: Titration and sorption measurements. *Journal of Contaminant Hydrology, 27*, 199–222.

Baeyens, B., & Bradbury, M. H. (2004). Cation exchange capacity measurements on illite using the sodium and cesium isotope dilution technique: Effects of the index cation, electrolyte concentration and competition: Modeling. *Clays and Clay Minerals, 52*, 421–431.

Barbier, F., Duc, G., & Petit-Ramel, M. (2000). Adsorption of lead and cadmium ions from aqueous solution to the montmorillonite/water interface. *Colloids and Surfaces A: Physicochemical and Engineering Aspects, 166*, 153–159.

Benson, L.V. (1980). Tabulation and evaluation of ion exchange data on smectites, certain zeolites and basalt (No.

https://doi.org/10.1007/s42860-021-00115-y Published online by Cambridge University Press

LBL-10541). California Univ., Berkeley (USA). Lawrence Berkeley Lab.

Berghout, A., Tunega, D., & Zaoui, A. (2010). Density functional theory (DFT) study of the hydration steps of Na^{+}/Mg^{2+}/Ca^{2+}/Sr^{2+}/Ba^{2+}-exchanged montmorillonites. *Clays and Clay Minerals, 58*, 174–187.

Bhattacharyya, K. G., & Gupta, S. S. (2008). Influence of acid activation on adsorption of Ni (II) and Cu (II) on kaolinite and montmorillonite: kinetic and thermodynamic study. *Chemical Engineering Journal, 136*, 1–13.

Bradbury, M. H., & Baeyens, B. (2005). Experimental measurements and modeling of sorption competition on montmorillonite. *Geochimica et Cosmochimica Acta, 69*, 4187–4197.

Charlet, L., & Tournassat, C. (2005). Fe (II)-Na (I)-Ca (II) cation exchange on montmorillonite in chloride medium: Evidence for preferential clay adsorption of chloride-metal ion pairs in seawater. *Aquatic Geochemistry, 11*, 115–137.

Chen, T., Yuan, Y., Zhao, Y., Rao, F., & Song, S. (2019). Preparation of montmorillonite nanosheets through freezing/thawing and ultrasonic exfoliation. *Langmuir, 35*, 2368–2374.

Chiou, C. T., & Rutherford, D. W. (1997). Effects of exchanged cation and layer charge on the sorption of water and EGME vapors on montmorillonite clays. *Clays and Clay Minerals, 45*, 867–880.

Cullen, J. T. & Maldonado, M. T. (2013). Biogeochemistry of cadmium and its release to the environment. Pp. 31–62 in: *Cadmium: From Toxicity to Essentiality* (A. Sigel, H. Sigel, and R. K.O. Sigel, editors). Springer, Dordrecht, Netherlands.

Davies, C. W. (1938). The extent of dissociation of salts in water. Part VIII. An equation for the mean ionic activity coefficient of an electrolyte in water, and a revision of the dissociation constants of some sulphates. *Journal of the Chemical Society*, *Part II*, 2093–2098.

Dazas, B., Ferrage, E., Delville, A., & Lanson, B. (2014). Interlayer structure model of tri-hydrated low-charge smectite by X-ray diffraction and Monte Carlo modeling in the Grand Canonical ensemble. *American Mineralogist, 99*, 1724–1735.

Di Leo, P., & Cuadros, J. (2003). ^{113}Cd, ^{1}H MAS NMR and FTIR analysis of Cd^{2+} adsorption on dioctahedral and trioctahedral smectite. *Clays and Clay Minerals, 51*, 403–414.

Dzene, L., Ferrage, E., Hubert, F., Delville, A., & Tertre, E. (2016). Experimental evidence of the contrasting reactivity of external vs. interlayer adsorption sites on swelling clay minerals: The case of Sr^{2+}-for-Ca^{2+} exchange in vermiculite. *Applied Clay Science, 132*, 205–215.

Efron, B. (1978). Regression and ANOVA with zero-one data: Measures of residual variation. *Journal of the American Statistical Association, 73*, 113–121.

Farrah, H., Hatton, D., & Pickering, W. F. (1980). The affinity of metal ions for clay surfaces. *Chemical Geology, 28*, 55–68.

Fehervari, A., Gates, W. P., Bouazza, A., & Shackelford, C. D. (2019). Assessment of bentonite compatibility with salinity using centrifugation-based water retention. *Geotechnical Testing Journal, 42*, 275–295.

Fernandes, M. M., & Baeyens, B. (2019). Cation exchange and surface complexation of lead on montmorillonite and illite including competitive adsorption effects. *Applied Geochemistry, 100*, 190–202.

Ferrage, E., Lanson, B., Sakharov, B. A., & Drits, V. A. (2005a). Investigation of smectite hydration properties by modeling experimental X-ray diffraction patterns: Part I. Montmorillonite hydration properties. *American Mineralogist, 90*, 1358–1374.

Ferrage, E., Tournassat, C., Rinnert, E., Charlet, L., & Lanson, B. (2005b). Experimental evidence for Ca-chloride ion pairs in the interlayer of montmorillonite. An XRD profile modeling approach. *Clays and Clay Minerals, 53*, 348–360.

Ferrage, E., Tournassat, C., Rinnert, E., & Lanson, B. (2005c). Influence of pH on the interlayer cationic composition and hydration state of Ca-montmorillonite: Analytical chemistry, chemical modelling and XRD profile modelling study. *Geochimica et Cosmochimica Acta, 69*, 2797–2812.

Fleischer, M. (1953). Recent estimates of the abundances of the elements in the earth's crust (No. 285). United States Department of the Interior, Geological Survey, Washington, D. C.

Fripiat, J. J., & Van Damme, H. (1983). Surface Mobility in Chemical Reactions and Catalysis. *Surface Mobilities on Solid Materials, Fundamental concepts and applications. NATO ASI Series B: Physics*, 86, 493-526. Springer, Boston, MA, USA.

Glaeser, R., & Méring, J. (1954). lsothermes d'hydratation des montmorillonites bi-ioniques (Na, Ca). *Clay Minerals Bulletin, 2,* 188–193.

Gu, X., Evans, L. J., & Barabash, S. J. (2010). Modeling the adsorption of Cd (II), Cu (II), Ni (II), Pb (II) and Zn (II) onto montmorillonite. *Geochimica et Cosmochimica Acta, 74*, 5718–5728.

Holmboe, M., Wold, S., & Jonsson, M. (2012). Porosity investigation of compacted bentonite using XRD profile modeling. *Journal of Contaminant Hydrology, 128,* 19–32.

Iwasaki, T., & Watanabe, T. (1988). Distribution of Ca and Na ions in dioctahedral smectites and interstratified dioctahedral mica/smectites. *Clays and Clay Minerals, 36*, 73–82.

Jacquier, P., Ly, J., & Beaucaire, C. (2004). The ion-exchange properties of the Tournemire argillite: I. Study of the H, Na, K, Cs, Ca and Mg behaviour. *Applied Clay Science, 26*, 163–170.

Jones, J. B., Jr. (2012). *Plant Nutrition and Soil Fertility Manual*. . CRC Press, Boca Raton, Florida, USA

Kaufhold, S., & Dohrmann, R. (2008). Detachment of colloidal particles from bentonites in water. *Applied Clay Science, 39*, 50–59.

Kaufhold, S., Dohrmann, R., Stucki, J. W., & Anastácio, A. S. (2011). Layer charge density of smectites–closing the gap between the structural formula method and the alkyl ammonium method. *Clays and Clay Minerals, 59*, 200–211.

Klika, Z., Kraus, L., & Vopálka, D. (2007). Cesium uptake from aqueous solutions by bentonite: A comparison of multicomponent sorption with ion-exchange models. *Langmuir, 23*, 1227–1233.

Kravchenko, J., Darrah, T. H., Miller, R. K., Lyerly, H. K., & Vengosh, A. (2014). A review of the health impacts of barium from natural and anthropogenic exposure. *Environmental Geochemistry and Health, 36*, 797–814.

Lagoutine, F., Legrand, J., & Bac, C. (1978). Half-lives of some radionuclides. *International Journal of Applied Radiation and Isotopes, 29*, 269–272.

Laird, D. A. (2006). Influence of layer charge on swelling of smectites. *Applied Clay Science, 34*, 74–87.

https://doi.org/10.1007/s42860-021-00115-y Published online by Cambridge University Press

Laudelout, H., Van Bladel, R., Bolt, G. H., & Page, A. L. (1968). Thermodynamics of heterovalent cation exchange reactions in a montmorillonite clay. *Transactions of the Faraday Society, 64*, 1477–1488.

Levy, R., & Francis, C. W. (1975). A quantitative method for the determination of montmorillonite in soils. *Clays and Clay Minerals, 23*, 85–89.

Li, W. Y. & Schulthess, C. P. (2020). Ion-exchange modeling of monovalent alkali cation adsorption on Montmorillonite. *Clays and Clay Minerals*, *68*, 476–490

Li, W. Y., Schulthess, C. P., Co, K., Sahoo, S., & Alpay, S. P. (2020). Influence of octahedral cation distribution in montmorillonite on interlayer hydrogen counter-ion retention strength by DFT simulation. *Clays and Clay Minerals*, 1-10.

Libby, W. F. (1956). Radioactive fallout and radioactive strontium. *Science, 123*, 657–660.

Mamy, J., & Gaultier, J. P. (1979). Etude comparee de l'evolution des montmorillonites biioniques K-Ca de Camp-Berteaux et du Wyoming sous l'effet des cycles d'humectation et de dessiccation. *Clay Minerals, 14*, 181–192.

Martin, L. A., Wissocq, A., Benedetti, M. F., & Latrille, C. (2018). Thallium (Tl) sorption onto illite and smectite: Implications for Tl mobility in the environment. *Geochimica et Cosmochimica Acta, 230*, 1–16.

Milodowski, A. E., Norris, S., & Alexander, W. R. (2016). Minimal alteration of montmorillonite following long-term interaction with natural alkaline groundwater: Implications for geological disposal of radioactive waste. *Applied Geochemistry, 66*, 184–197.

Missana, T., Benedicto, A., García-Gutiérrez, M., & Alonso, U. (2014). Modeling cesium retention onto Na-, K-and Ca-smectite: Effects of ionic strength, exchange and competing cations on the determination of selectivity coefficients. *Geochimica et Cosmochimica Acta, 128*, 266–277.

Missana, T., & García-Gutiérrez, M. (2007). Adsorption of bivalent ions (Ca (II), Sr (II) and Co (II)) onto FEBEX bentonite. *Physics and Chemistry of the Earth, Parts A/B/C, 32*, 559–567.

Molera, M., Eriksen, T. & Wold, S. (2002). Modeling strontium sorption in natural and purified bentonite clay. *TRePro workshop of the Forschungszentrum Karlsruhe, March 2002: Modelling of Coupled Transport Reaction Processes*. 60-64.

Montemore, M. M., van Spronsen, M. A., Madix, R. J., & Friend, C. M. (2017). O_2 activation by metal surfaces: Implications for bonding and reactivity on heterogeneous catalysts. *Chemical Reviews, 118,* 2816–2862.

Morodome, S., & Kawamura, K. (2011). In situ X-ray diffraction study of the swelling of montmorillonite as affected by exchangeable cations and temperature. *Clays and Clay Minerals, 59*, 165–175.

Motellier, S., Ly, J., Gorgeon, L., Charles, Y., Hainos, D., Meier, P., & Page, J. (2003). Modelling of the ion-exchange properties and indirect determination of the interstitial water composition of an argillaceous rock. Application to the Callovo-Oxfordian low-water-content formation. *Applied Geochemistry, 18*, 1517–1530.

Nash, V. E. & Marshall, C. E. (1956). *The Surface Reactions of Silicate Minerals: The Reactions of Feldspar Surfaces with Acidic Solutions.* Agricultural Experiment Station, College of Agriculture, University of Missouri, USA, *Bulletin* 613.

Nilsson, A., & Book, S. A. (1987). Occurrence and distribution of bone tumors in beagle dogs exposed to ^{90}Sr. *Acta Oncologica, 26*, 133–138.

Nolin, D. (1997). Rétention de radioéléments à vie longue par des matériaux argileux. Influence d'anions contenus dans les eaux naturelles. Ph.D. dissertation, Universite Pierre et Marie Curie, Paris 6, France.

Nordberg, G. F. (2004). Cadmium and health in the 21st century–historical remarks and trends for the future. *Biometals, 17*, 485–489.

Norrish, K., & Quirk, J. P. (1954). Crystalline swelling of montmorillonite: Use of electrolytes to control swelling. *Nature, 173*, 255–256.

Oueslati, W., Rhaiem, H. B., & Amara, A. B. H. (2011). XRD investigations of hydrated homoionic montmorillonite saturated by several heavy metal cations. *Desalination, 271,* 139–149.

Oueslati, W., Rhaiem, H. B., & Amara, A. B. H. (2012). Effect of relative humidity constraint on the metal exchanged montmorillonite performance: An XRD profile modeling approach. *Applied Surface Science, 261,* 396–404.

Oueslati, W., Chorfi, N., & Abdelwahed, M. (2017). Effect of mechanical constraint on the hydration properties of Na-montmorillonite: Study under extreme relative humidity conditions. *Powder Diffraction, 32*, S160–S167.

Peynet, V. (2003). Rétention d'actinides et de produits de fission par des phases solides polyminérales. Ph.D. dissertation, Universite Paris 6, France.

Pils, J. R., Laird, D. A., & Evangelou, V. P. (2007). Role of cation demixing and quasicrystal formation and breakup on the stability of smectitic colloids. *Applied Clay Science, 35*, 201–211.

Poli, A. L., Batista, T., Schmitt, C. C., Gessner, F., & Neumann, M. G. (2008). Effect of sonication on the particle size of montmorillonite clays. *Journal of Colloid and Interface Science, 325*, 386–390.

Pinot, F., Kreps, S. E., Bachelet, M., Hainaut, P., Bakonyi, M., & Polla, B. S. (2000). Cadmium in the environment: Sources, mechanisms of biotoxicity, and biomarkers. *Reviews on Environmental Health, 15*, 299–324.

Reijonen, H. M., & Alexander, W. R. (2015). Bentonite analogue research related to geological disposal of radioactive waste: Current status and future outlook. *Swiss Journal of Geosciences, 108*, 101–110.

Robin, V., Tertre, E., Beaucaire, C., Regnault, O., & Descostes, M. (2017). Experimental data and assessment of predictive modeling for radium ion-exchange on beidellite, a swelling clay mineral with a tetrahedral charge. *Applied Geochemistry, 85*, 1–9.

Robin, V., Tertre, E., Beaufort, D., Regnault, O., Sardini, P., & Descostes, M. (2015). Ion exchange reactions of major inorganic cations (H^+, Na^+, Ca^{2+}, Mg^{2+} and K^+) on beidellite: Experimental results and new thermodynamic database. Toward a better prediction of contaminant mobility in natural environments. *Applied Geochemistry, 59*, 74–84.

Salles, F., Bildstein, O., Douillard, J. M., Jullien, M., & Van Damme, H. (2007). Determination of the driving force for the hydration of the swelling clays from computation of the hydration energy of the interlayer cations and the

https://doi.org/10.1007/s42860-021-00115-y Published online by Cambridge University Press

clay layer. *The Journal of Physical Chemistry C, 111*, 13170–13176.

Salles, F., Douillard, J. M., Bildstein, O., Gaudin, C., Prelot, B., Zajac, J., & Van Damme, H. (2013). Driving force for the hydration of the swelling clays: Case of montmorillonites saturated with alkaline-earth cations. *Journal of Colloid and Interface Science, 395*, 269–276.

Savoye, S., Beaucaire, C., Grenut, B., & Fayette, A. (2015). Impact of the solution ionic strength on strontium diffusion through the Callovo-Oxfordian clayrocks: An experimental and modeling study. *Applied Geochemistry, 61*, 41–52.

Schatzberg, P. (1967). Molecular diameter of water from solubility and diffusion measurements. *The Journal of Physical Chemistry, 71,* 4569–4570.

Schoonheydt, R. A., Johnston, C. T., Brigatti, M. F. & Mottana, A. (2011). The surface properties of clay minerals. Pp. 337–373 in: *Layered Structures and their Application in Advanced Technologies* (M.F. Brigatti and A. Mottana, editors). EMU Notes in Mineralogy, **11**, European Mineralogical Union and the Mineralogical Society of Great Britain & Ireland.

Schulthess, C. P. (2005). *Soil Chemistry with Applied Mathematics.* Trafford, Victoria, British Columbia, Canada.

Schulthess, C. P., & Huang, C. P. (1990). Adsorption of heavy metals by silicon and aluminum oxide surfaces on clay minerals. *Soil Science Society of America Journal, 54*, 679–688.

Schulthess, C. P., Taylor, R. W., & Ferreira, D. R. (2011). The nanopore inner sphere enhancement effect on cation adsorption: Sodium and nickel. *Soil Science Society of America Journal, 75*, 378–388.

Siroux, B., Beaucaire, C., Tabarant, M., Benedetti, M. F., & Reiller, P. E. (2017). Adsorption of strontium and caesium onto an Na-MX80 bentonite: Experiments and building of a coherent thermodynamic modelling. *Applied Geochemistry, 87*, 167–175.

Smith, D. W. (1977). Ionic hydration enthalpies. *Journal of Chemical Education, 54*, 540.

Starichenko, V. I. (2011). Accumulation of ^{90}Sr in the bone tissue of northern mole voles in the head portion of the East Ural Radioactive Trace. *Russian Journal of Ecology, 42*, 64–70.

Tajeddine, L., Gailhanou, H., Blanc, P., Lassin, A., Gaboreau, S., & Vieillard, P. (2015). Hydration–dehydration behavior and thermodynamics of MX-80 montmorillonite studied using thermal analysis. *Thermochimica Acta, 604*, 83–93.

Teppen, B. J., & Miller, D. M. (2006). Hydration energy determines isovalent cation exchange selectivity by clay minerals. *Soil Science Society of America Journal, 70*, 31–40.

Tertre, E., Beaucaire, C., Coreau, N., & Juery, A. (2009). Modelling Zn (II) sorption onto clayey sediments using a multi-site ion-exchange model. *Applied Geochemistry, 24*, 1852–1861.

Tertre, E., Ferrage, E., Bihannic, I., Michot, L. J., & Prêt, D. (2011). Influence of the ionic strength and solid/solution ratio on Ca (II)-for-Na^+ exchange on montmorillonite. Part 2: Understanding the effect of the m/V ratio. Implications for pore water composition and element transport in natural media. *Journal of Colloid and Interface Science, 363*, 334–347.

The Clay Mineral Society (2020). Physical and chemical data of source clays, http://www.clays.org/sourceclays_data.html, viewed 2 November 2020.

Tournassat, C., Neaman, A., Villiéras, F., Bosbach, D., & Charlet, L. (2003). Nanomorphology of montmorillonite particles: Estimation of the clay edge sorption site density by low-pressure gas adsorption and AFM observations. *American Mineralogist, 88*, 1989–1995.

Tournassat, C., Ferrage, E., Poinsignon, C., & Charlet, L. (2004a). The titration of clay minerals: II. Structure-based model and implications for clay reactivity. *Journal of Colloid and Interface Science, 273*, 234–246.

Tournassat, C., Greneche, J. M., Tisserand, D., & Charlet, L. (2004b). The titration of clay minerals: I. Discontinuous backtitration technique combined with CEC measurements. *Journal of Colloid and Interface Science, 273*, 224–233.

Tournassat, C., Bizi, M., Braibant, G., & Crouzet, C. (2011). Influence of montmorillonite tactoid size on Na–Ca cation exchange reactions. *Journal of Colloid and Interface Science, 364*, 443–454.

Van Spronsen, M. A., Frenken, J. W., & Groot, I. M. (2017). Observing the oxidation of platinum. *Nature Communications, 8,* 1–7.

Wissocq, A., Beaucaire, C., & Latrille, C. (2018). Application of the multi-site ion exchanger model to the sorption of Sr and Cs on natural clayey sandstone. *Applied Geochemistry, 93*, 167–177.

Xia, M., Jiang, Y., Zhao, L., Li, F., Xue, B., Sun, M., Liu, D., & Zhang, X. (2010). Wet grinding of montmorillonite and its effect on the properties of mesoporous montmorillonite. *Colloids and Surfaces A: Physicochemical and Engineering Aspects, 356*, 1–9.

Yu, S., Mei, H., Chen, X., Tan, X., Ahmad, B., Alsaedi, A., Hayat, T. & Wang, X. (2015). Impact of environmental conditions on the sorption behavior of radionuclide ^{90}Sr (II) on Na-montmorillonite. *Journal of Molecular Liquids*, *203*, 39-46.

(Received 23 July 2020; revised 12 February 2021; AE: Reiner Dohrmann)

https://doi.org/10.1007/s42860-021-00115-y Published online by Cambridge University Press